NASA CONTRACTOR REPORT

NASA CR-2166

NASA CR-2166

FAILURE ANALYSIS OF ALUMINUM ALLOY COMPONENTS

by Om Johari, Irene Corvin, and Joseph Staschke

Prepared by
IIT RESEARCH INSTITUTE
Chicago, Ill. 60616
for Langley Research Center

NATIONAL AERONAUTICS AND SPACE ADMINISTRATION • WASHINGTON, D. C. • JANUARY 1973

1. Report No.	2. Government Accession No.	3. Recipient's Catalog No.
NASA CR-2166		

4. Title and Subtitle	5. Report Date
Failure Analysis of Aluminum Alloy Components	January 1973
	6. Performing Organization Code

7. Author(s)	8. Performing Organization Report No.
Dr. Om Johari, Irene Corvin, and Joseph Staschke	IITRI-B6114-7
	10. Work Unit No.

9. Performing Organization Name and Address	11. Contract or Grant No.
IIT Research Institute 10 West 35 Street Chicago, Illinois 60616	NAS1-10788
	13. Type of Report and Period Covered

12. Sponsoring Agency Name and Address	13. Type of Report and Period Covered
National Aeronautics and Space Administration Washington, D. C. 20546	Final Rep.6/1/71-4/15/72
	14. Sponsoring Agency Code

15. Supplementary Notes

The samples for this program were provided by Mr. B. Cohen and Mr. R. L. Henderson of Air Force Materials Laboratory, Mr. Sam Goldberg of Naval Air Systems Command, and Mr. W. Sipes of Naval Air Development Center.

16. Abstract

Analysis of six service failures in aluminum alloy components which failed in aerospace applications is reported. Identification of fracture surface features from fatigue and overload modes was straightforward, though the specimens were not always in a clean, smear-free condition most suitable for failure analysis. The presence of corrosion products and of chemically attacked or mechanically rubbed areas here hindered precise determination of the cause of crack initiation, which was then indirectly inferred from the scanning electron fractography results. In five failures the crack propagation was by fatigue, though in each case the fatigue crack initiated from a different cause. Some of these causes could be eliminated in future components by better process control. In one failure, the cause was determined to be impact during a crash--the features of impact fracture were distinguished from overload fractures by direct comparisons of the received specimens with laboratory-generated failures.

17. Key Words (Suggested by Author(s))	18. Distribution Statement
Failure Analysis, Fatigue Scanning Electron Microscopy, Fractography, Metallography Aluminum Alloys, Failure Prevention Aircraft components, Shot peening	

19. Security Classif. (of this report)	20. Security Classif. (of this page)	21. No. of Pages	22. Price*
Unclassified	Unclassified	71	$3.00

*For sale by the National Technical Information Service, Springfield, Virginia 22151

TABLE OF CONTENTS

FAILURE ANALYSIS OF ALUMINUM ALLOY COMPONENTS

By Om Johari, Irene Corvin, and Joseph Staschke
IIT Research Institute

SUMMARY

This program consisted of the failure analysis of six aluminum alloy components which failed in aerospace applications. The six reports detailing the failure analysis are appended. The highlights of the findings and conclusions are presented below.

(1) The results and discussions well document the important role played by scanning electron microscopy in failure analysis. All of its important advantages--namely, directness, large depth of focus, broad range of available magnifications, and analytical capability via X-ray spectroscopy--proved most valuable in performing the observations. Although no stereo-pairs are presented in this report, many were taken, and they aided greatly in the interpretation of results. Our experience from this program indicates that frequent use of X-ray analysis and stereo-pairs with the SEM is essential in failure studies.

(2) In aluminum alloy samples examined here, fatigue features were not difficult to locate; thus, five failures could readily be attributed to fatigue. The origin of the fatigue cracking could also be located, but the specimen condition hindered identification of the precise cause of crack initiation. Based on detailed analysis, however, the possible origin could be indirectly inferred. It appears that the damage due to (a) maximum rubbing and smearing at this location, and (b) maximum attack from the environment is intensified at the origin area which is exposed for the longest time. Additional work in various aspects of specimen cleaning may provide new approaches in pinpointing the cause, but at present, in most service failures cause of origin presents the most challenging task and, at best, must be determined from indirect analysis of results.

In preventing future failures, lessons learned from one failure must be applied to other components. Thus, determination of the precise cause of initiation has considerable value; however, as the results show, much valuable information can be indirectly obtained by analysis of results from fracture surfaces, in combination with the metallography and specimen surface condition studies. Using this approach improper control during shot peening could be determined as the cause of failure in a shot-peened component; in a forged component having a processing flaw, the possible origin of this crack-initiating defect could be attributed to initial casting; and the role of corrosion in initiating fracture and/or masking details of its origin could be determined.

(3) This work has pointed out some obvious and some not so obvious causes of failures. Thus, poorly controlled shot peening, lack of shot peening at thread roots, and presence of processing flaws resulted in failures as expected. These causes can be readily eliminated in future components by suggesting better process control. In other cases more background data may be required to suggest remedial action; e.g., if similar failures frequently occurred, a design or material change might be necessary.

(4) In all the fatigue specimens studied, overload features were readily identified and distinguished from fatigue features. While the fatigue features were used to determine the origin and direction of crack propagation, overload features were useful in determining the nature of the alloy--its cleanliness, directionality in working, etc.

(5) The overload regions also provide direct information about the microstructure of the alloy. In the work reported here, SEM metallography has been used exclusively, and the results of microstructure determination in SEM from both polished and fractured surfaces confirm the advantages previously cited (ref. 1).

(6) One of the specimens studied illustrates how a comparison type approach can be a valuable adjunct to failure analysis. Although fracture surface features depend on the nature of loading and environment, microstructure also has a very important effect. Thus, it is critical that either samples with similar microstructures be compared, or the role of microstructure be clearly understood. If the amount of material is sufficient, as was the case in the present work, this could be done by preparing representative test samples from the failed piece. This "handbook type" approach is demonstrated to be valuable in distinguishing impact and overload modes. Fatigue modes were readily identifiable, though experience gained from the handbook program (ref. 2) was helpful.

The nature of our results and their discussion warrant widespread circulation to be helpful in preventing failures and describing failure analysis approaches. Every effort will be made to publish these reports in journals and present them at meetings. The reports have been submitted to the American Society for Metals for inclusion in their failure analysis handbook.

APPENDIX I

FAILURE ANALYSIS OF ALUMINUM ALLOY COMPONENTS--SAMPLE I

1. INTRODUCTION

This report presents our analysis of an aluminum flap hinge fitting for NASA-Langley Research Center. The part was obtained from Air Force Materials Laboratory. The material was identified as 2024 aluminum alloy in the T6 condition, with a hardness of Rockwell B 80. The chemical analysis, as supplied by AFML, was as follows:

Cu	Si	Mn	Mg	Fe	Zn	Ti	Cr	Al
4.30	0.84	0.69	0.43	0.31	0.15	0.03	0.05	Bal.

The hinge flap had a crack in the center of the fillet area. This crack had been opened and analyzed by optical and transmission replica electron microscopy before shipment to IITRI. The sample in the as-received condition is shown in Fig. 1. A close-up of the area is shown in Fig. 2. This close-up, as well as information available on the sample from AFML, indicated it to be a fatigue crack.

2. EXPERIMENTAL METHOD

The sample was carefully cut to suitable size, cleaned in a trichloroethylene solution, and examined in the JSM-2 scanning electron microscope at a range of magnifications. Most of the SEM photographs were taken as stereo pairs.

3. RESULTS

Region A of Fig. 2 is magnified in Fig. 3. Even at this low magnification many fatigue features are evident. A close examination of this photograph shows many fatigue striations. SEM examination enabled the striations to be observed at this low magnification. Many other areas along the crescent-shaped edge showed similar features. Some typical areas are shown in Figs. 4 to 6. In addition, several high-magnification photographs illustrating the fatigue striations are presented in Figs. 7 to 9.

4. DISCUSSION

The crack started by fatigue although no specific origin could be found. Figures 3 to 6 suggest that there were probably many local sites and the cracks grew from each to form the appearance in Fig. 2. The specimen edge was subsequently polished and examined in an attempt to find specific clues as to the origin, but without success. The possibility of inclusion-initiated origin is thus ruled out, though surface defect (scratch) or local overload may have initiated the failure. These hypotheses would be verified if similar cracks are found in other flap hinges.

The identification of striations so close to the crack initiation sites is interpreted to suggest that the crack was due to low cycle-high load fatigue. In all cases examined for high cycle fatigue in aluminum alloys included in the Fracture Handbook Program,[2] striations were not identified at these low magnifications and so close to the initiation sites.

The results clearly illustrate the value of SEM in failure analysis. The large depth of focus and the low magnification permitted a large area of the sample to be rapidly examined without any specimen preparation. The important fracture features, namely striations, could also be identified at relatively low magnification. While total analysis could not be carried out with optical microscopy, replica preparation and examination in the transmission electron microscope allows this failure analysis also. However, the detailed and complete information obtainable by TEM would require considerably more time and effort as compared to SEM examination. The SEM-TEM comparison for failure analysis as described previously[3] is thus well illustrated by this example.

5. CONCLUSION

The fatigue crack was initiated at many sites along the center of the fillet. The results suggest that it was a low-cycle fatigue failure.

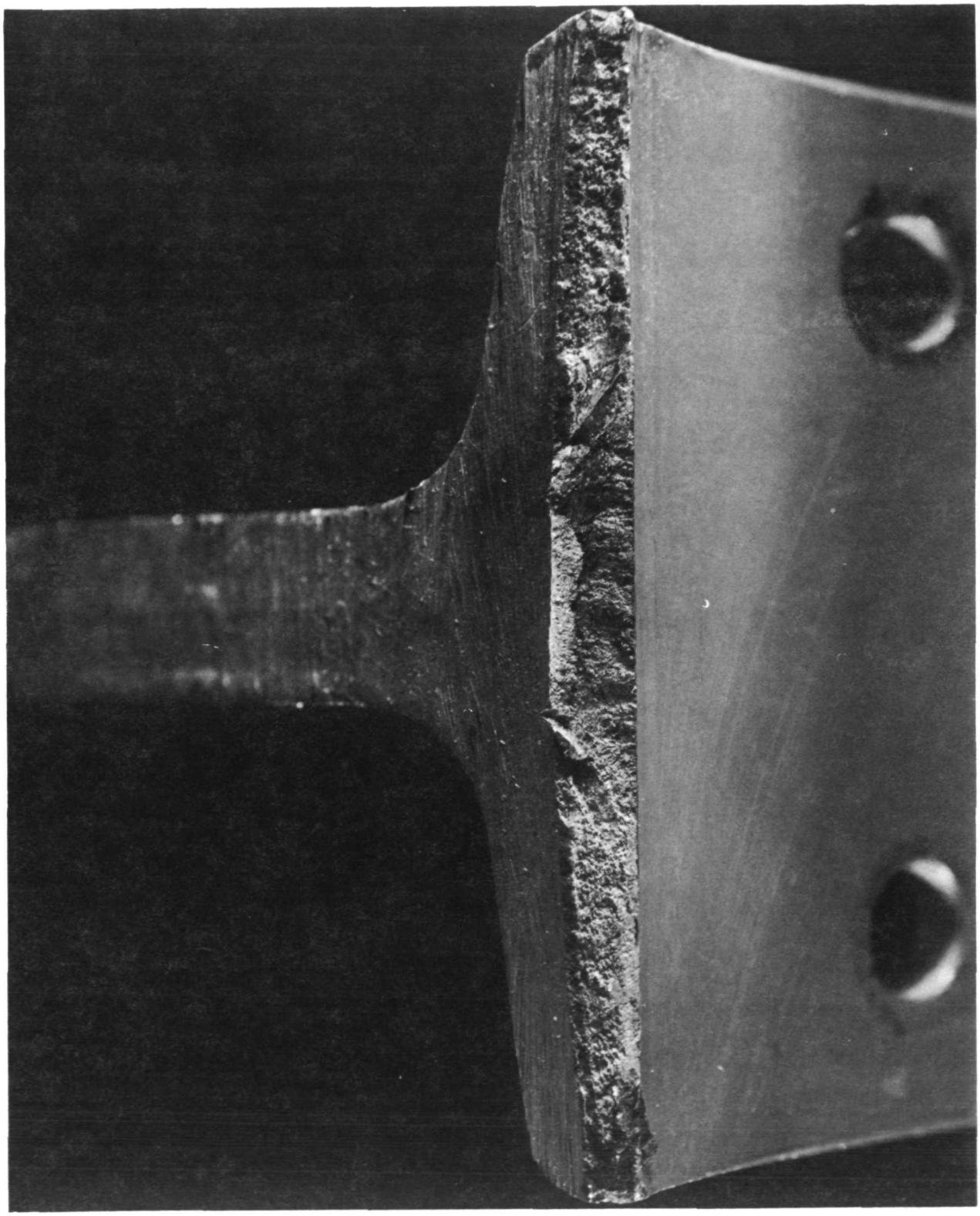

Figure 1 Mag. 4X

Overview of Failed Aluminum Flap Hinge Fitting in the As-Received Condition.

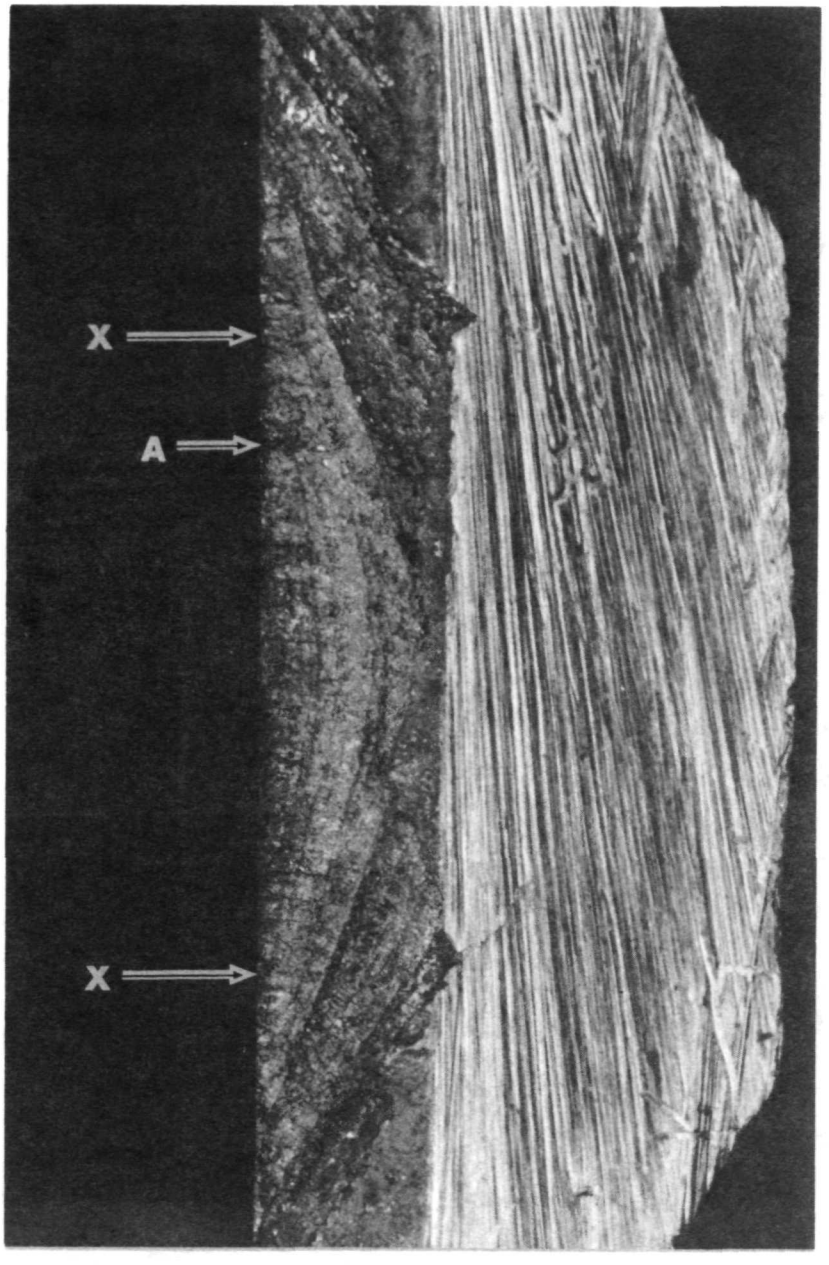

Mag. 11X

Fig. 2

Photomacrograph of the Fracture Surface, Showing the Fatigue-Initiated Fracture Face Appearance.

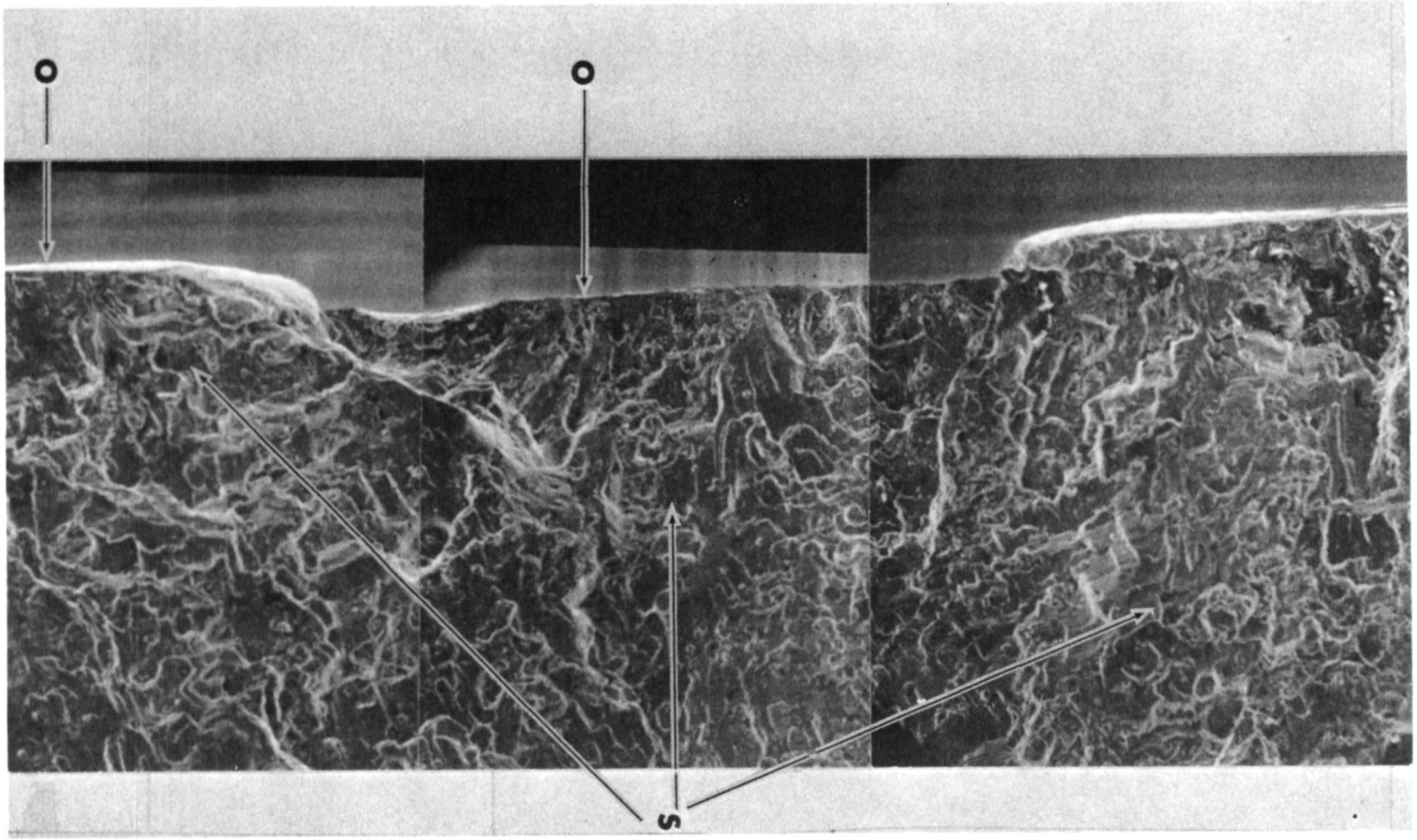

Mag. 135X

Fig. 3

Composite Photograph of Region A in Fig. 2. Notice the presence of striations at areas S. This photo suggests that areas O could be possible origin.

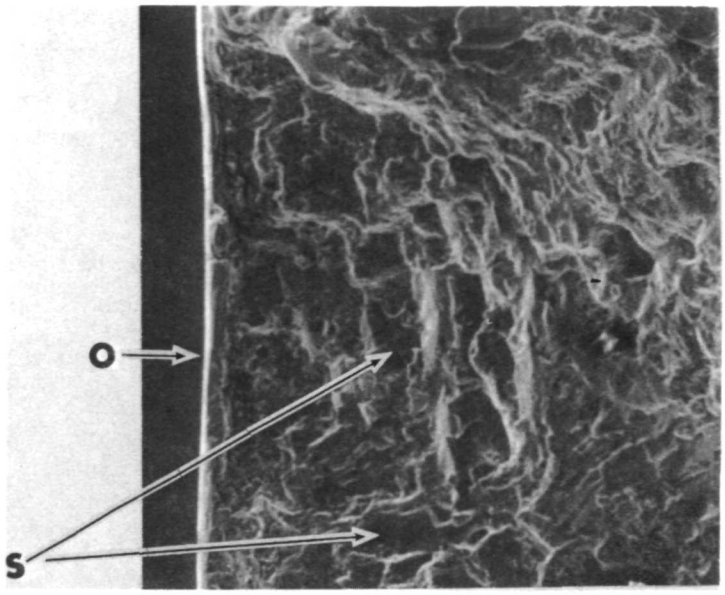

Mag. 155X

Fig. 4

Another Region Close to the Edge. Areas S again show striations. Region O could be another possible origin.

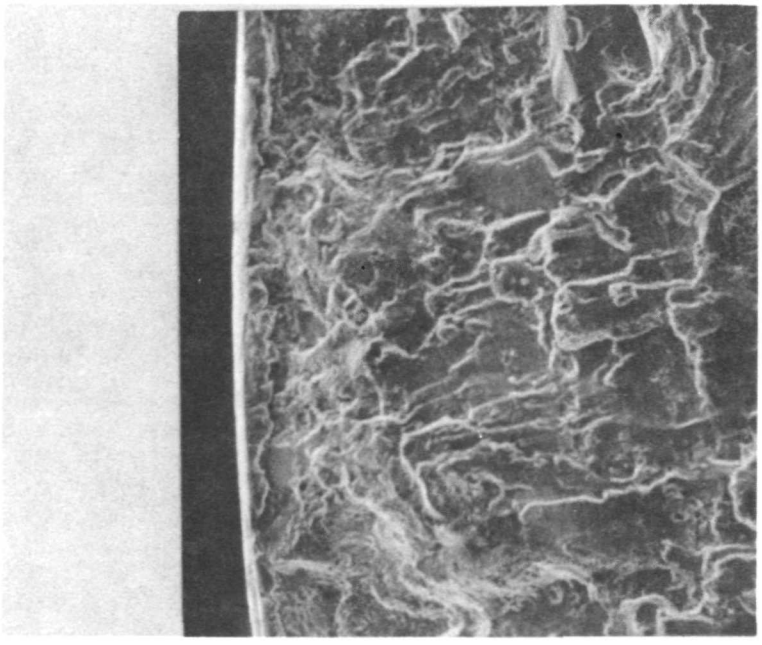

Mag. 230X

Fig. 5

Another Possible Initiation Site. Notice the ease with which striations can be discerned at this low magnification.

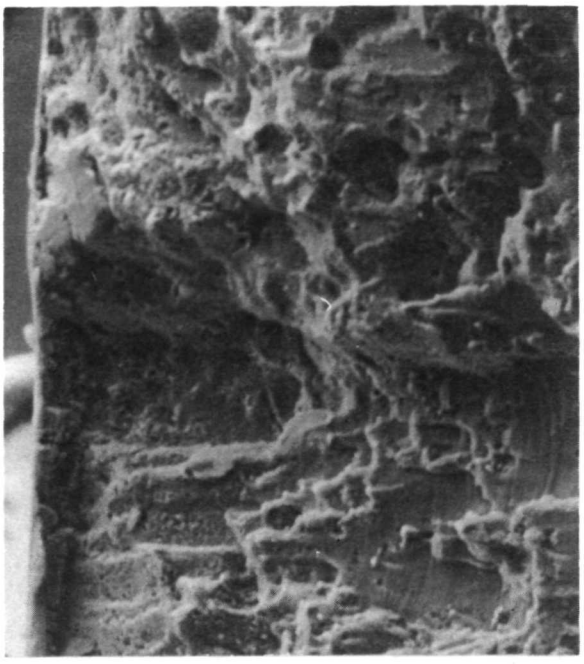

Mag. 200X

Fig. 6

Yet Another Possible Initiation Site. Many such regions were identified all along the region XX of Fig. 3.

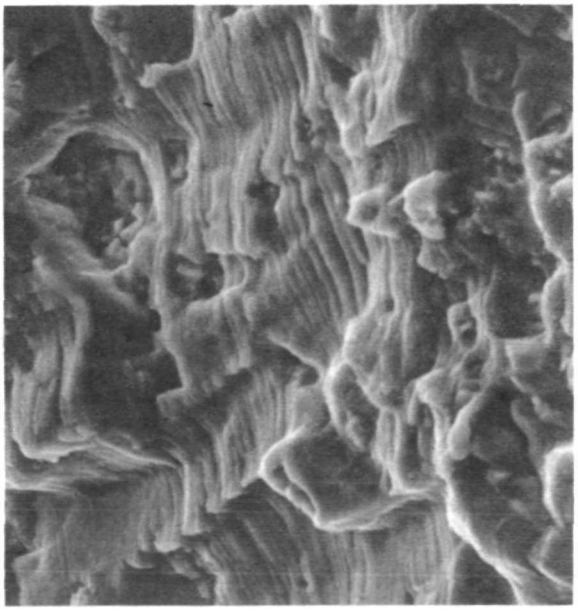

Mag. 600X

Fig. 7

Fatigue Striations at Higher Magnification.

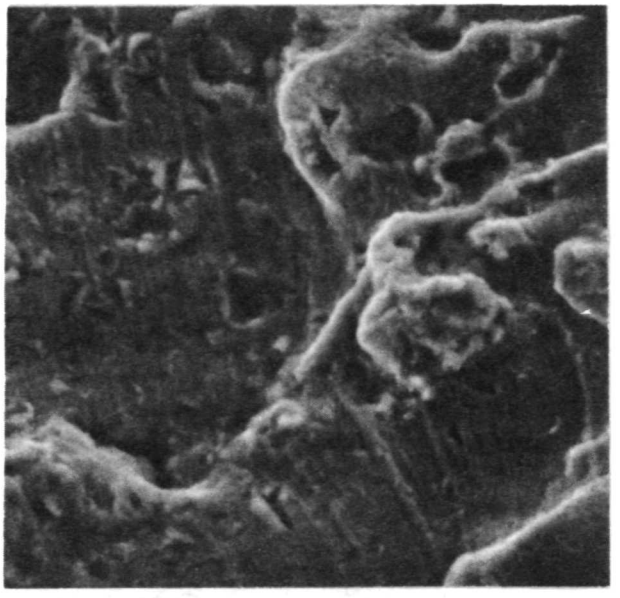

Mag. 1540X

Fig. 8

Fatigue Striations in Another Region.

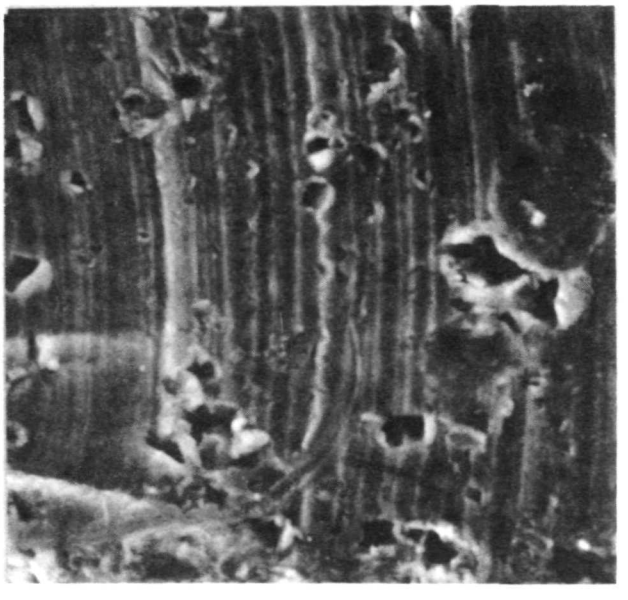

Mag. 2300X

Fig. 9

Another Region Showing Fatigue Striations.

APPENDIX II

FAILURE ANALYSIS OF ALUMINUM ALLOY COMPONENTS--SAMPLE II

1. INTRODUCTION

This report presents our analysis of an aluminum shock strut piston failure in a naval aircraft. The part was obtained from the Naval Air Development Center (NADC), Johnsville, Pa., where it had been forwarded from the Naval Air Rework Facility at Norfolk, Va. The material was identified as 7075 aluminum alloy heat-treated to the T6 condition. The hardness of the failed part was Rockwell B 80.

Before receipt of the sample at IIT Research Institute it had been analyzed by the NADC using optical and replica transmission electron fractography.[4] Figure 1 shows the overall fracture surface, and Fig. 2 shows the elevation view of the failed piston.[4] Figure 3 presents an overall view of the part as received by IITRI. We did not have access to the other half of the fracture. Close-ups of areas 1 and 3, as shown in Figs. 4 and 5, were examined in detail. A cursory examination of areas 2 and 4 indicated them to be identical to 1 and 3. The identification of fracture mode was not possible from optical macrofractographs alone. The information provided by NADC indicated it to be a fatigue failure.[4]

2. EXPERIMENTAL METHOD

Specimens of interest were cut from the as-received part (Fig. 3). These specimens were cleaned ultrasonically in trichloroethylene, although some parts of the speicmens did not clean up even after repeated ultrasonic immersions. The specimens were examined in a JSM-2 scanning electron microscope at a range of magnifications. Many of the photographs were taken as stereo-pairs.

3. RESULTS

The results are presented in two parts: the first, dealing with examaination of the suspect origin regions; the second, with the surrounding areas.

3.1 Suspect Origin Regions

Figure 6 presents a composite photograph of area 3. Figure 7 is a higher magnification view of the center of the region SS of Fig. 6. Four distinct regions are identified, and in this report they are termed A, B, C, and D--A being closest to the outside shot-peened surface, D being the final fracture overload region. Typical features of region D are illustrated in Fig. 8a and 8b. Regions B and C were clearly separated because, both in high-magnification optical macrofractographs (Fig. 9) and in SEM photographs, region B was much darker than region C. Typical fatigue striations could be readily observed in region C. The direction of striations pointed towards the center of the area SS as the origin, though local effects of grain orientations were also observed (Fig. 10 a, b, c). Except towards the edges of the crescent SS (as shown in Fig. 10), the striations, for the most part, were parallel to the circumference of the ring-shaped sample.

Figure 11a and 11b shows that the boundary between regions B and C is clearly separated. In general, region B was heavily contaminated; the film which was present could not be removed by repeated ultrasonic cleaning. The structure of the contaminants is clearly brought out at high magnification in Fig. 12. Figure 13 presents a comparison between regions B and C. The fatigue features can be seen at some locations in region B, but at most locations the features are totally obscured due to being covered by the contaminants.

In region A, no specific initiation point could be found; Fig. 14 is a high-magnification photograph of this region. Grain boundaries were separated and were clearly identified in most areas of region A. The structure here appears to have been induced by chemical attack (Fig. 15).

3.2 Areas Around Suspect-Origin Region

In the area outside the suspect-origin region described above (i.e., outside the region SS of Fig. 6) four similar regions were observed (Fig. 16 a, b). The features of regions C and D were identical. In all areas of regions B and C the striations were parallel to the circumference of the sample (Figs. 17 and 18). The darker region B (Fig. 17 a, b) was again more contaminated than region C, and though fatigue features are suspected, they could not be clearly resolved. In Fig. 18 a, b, and c the boundary between B and C is, again, very distinct. Area A (Fig. 19 a, b) is also very similar in the regions inside and outside SS of Fig. 6.

4. DISCUSSION

Based on the above results, it is established that the mechanism of failure was fatigue and the final fracture was by overload. Region C showed fatigue striations at all locations around the circumference of the fracture face more clearly than region B, although some fatigue features were observed in region B also. Since the component is a shock strut, this evidence suggests that, after the crack propagated to the end of region B, either it stopped for a considerable length of time or the strut was exposed to a hostile environment allowing contamination to build up on the opened crack. Many possible sources of this contamination, as well as the chemical attack observed at region A, could be encountered by the strut during its use on a naval aircraft. The crack propagation in regions C and D leading to final fracture possibly occurred during a shorter period of service or was in a less hostile environment so that this area remained relatively free of contamination.

The identical nature of A areas (Figs. 14 and 19) in SS regions (there were at least five such regions at various points on the circumference of the section received) and outside SS is attributed to (1) continuous rubbing and smearing in this area which fractured first, and (2) chemical attack resulting from exposure to corrosive environments during the life of the

part since this area, being closest to the specimen surface, suffers maximum exposure. Also, alkaline solutions are used to clean aluminum alloy components, and the structure in Figs. 14 and 19 could arise from the use of such solutions before the crack opened beyond the initial stages of region B.

No specific cause of fracture origin could be established from the above observations. The crescent-shaped regions always occurred in a plane below the minimum cross-section plane containing most of the fracture. The specimen had been shot-peened, and a study of the shot-peened surface revealed many defects; some areas showed surface cracks and many areas showed original machine markings suggesting improper control of shot-peening parameters (Fig. 20).

Region A in the areas observed (e.g., Figs. 7 and 16) extends to approximately 0.025 cm below the shot-peened surface. Since shot peening is employed to prevent fatigue failures by providing compressive stresses at the immediate surface (usually the first 0.013 cm or less), observations such as in Fig. 20 indicate that many areas were either not hit or very lightly hit by the shots and derived no benefit from the shot-peening operations. Large isolated areas of unfavorable stress states caused by poorly controlled shot peening and located at or near the minimum section of the strut could thus act as initiation sites. The observations of many suspect initiation sites support this explanation, although precise correlation between any surface defects and fatigue initiation sites was not found.

To futher verify the shot peening damage a metallographic section was prepared (Figs. 21 and 22). Detailed SEM examination of this section (Fig. 23) revealed presence of many flaws and confirmed the uneven nature of shot-peening load distributions.

The following failure mechanism is proposed based on the above results and discussion. Sipes[4] had proposed a similar mechanism and, in that respect, our results and conclusions, based on definite experimental evidence observable only by SEM,

support Sipes' hypothesis. The crack initiated at amny surface defects (probably shot-peening defects, with or without machining defects) and propagated to the end of region A. The changed stress state then caused the cracks from these locations to propagate along the circumference until they met, and the entire A region was opened up exhausting any beneficial effects of shot peening. This could have been confirmed by presence of radial striations in areas A, but except for two isolated observations, the smeared and chemically attacked condition of region A prevented such confirmation. Following this, the crack propagated by fatigue during each loading cycle, opening up more and more of the specimen cross-section (through regions B and C) until a critical cross-section was reached, at which time the strut was no longer able to support the load and final fracture occurred by overload.

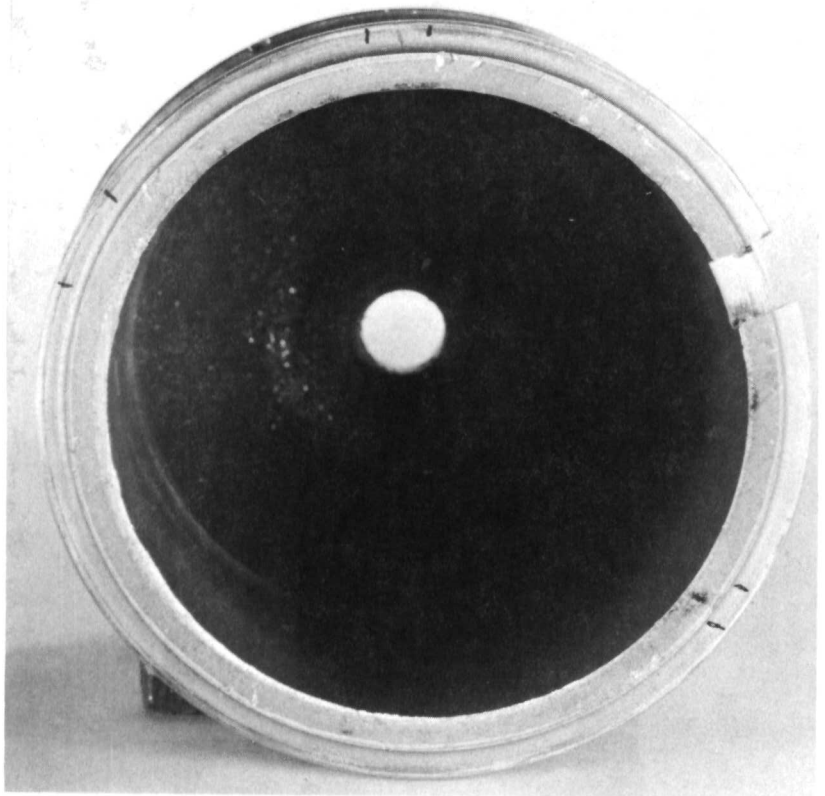

Figure 1

Plan View of Failed Aluminum
Shock Strut Piston
(Courtesy Naval Air Development Center)

Figure 2

Elevation View of the Failed Piston
(Courtesy Naval Air Development Center)

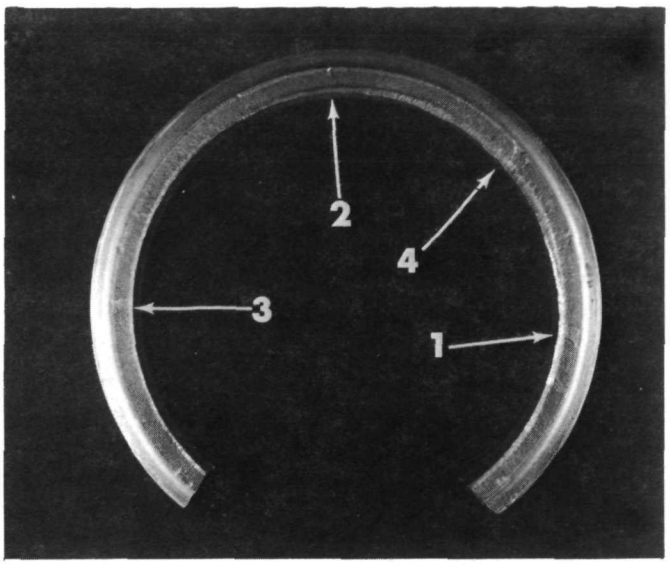

Figure 3

Failed Part in the As-Received Condition
by IITRI Indicating Areas Examined.

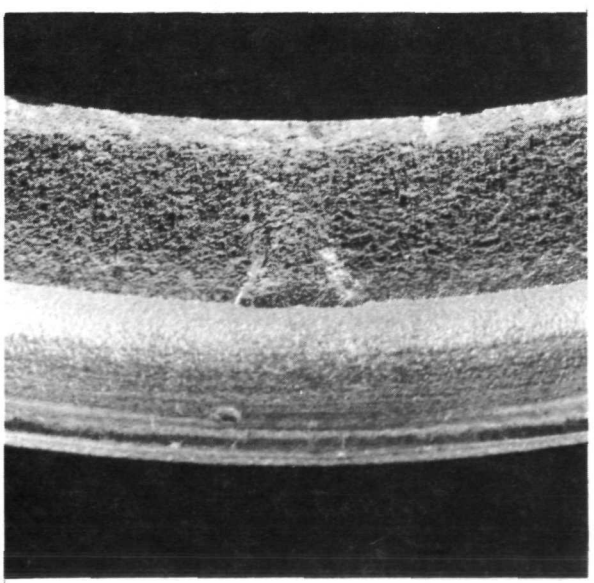

Mag. 5X

Figure 4

Close-Up of Area 1 in Figure 3.

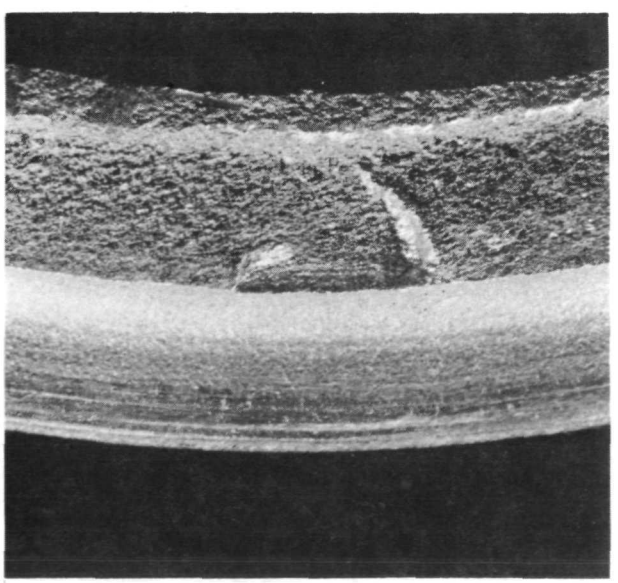

Mag. 5X

Figure 5

Close-Up of Area 3 in Figure 3.

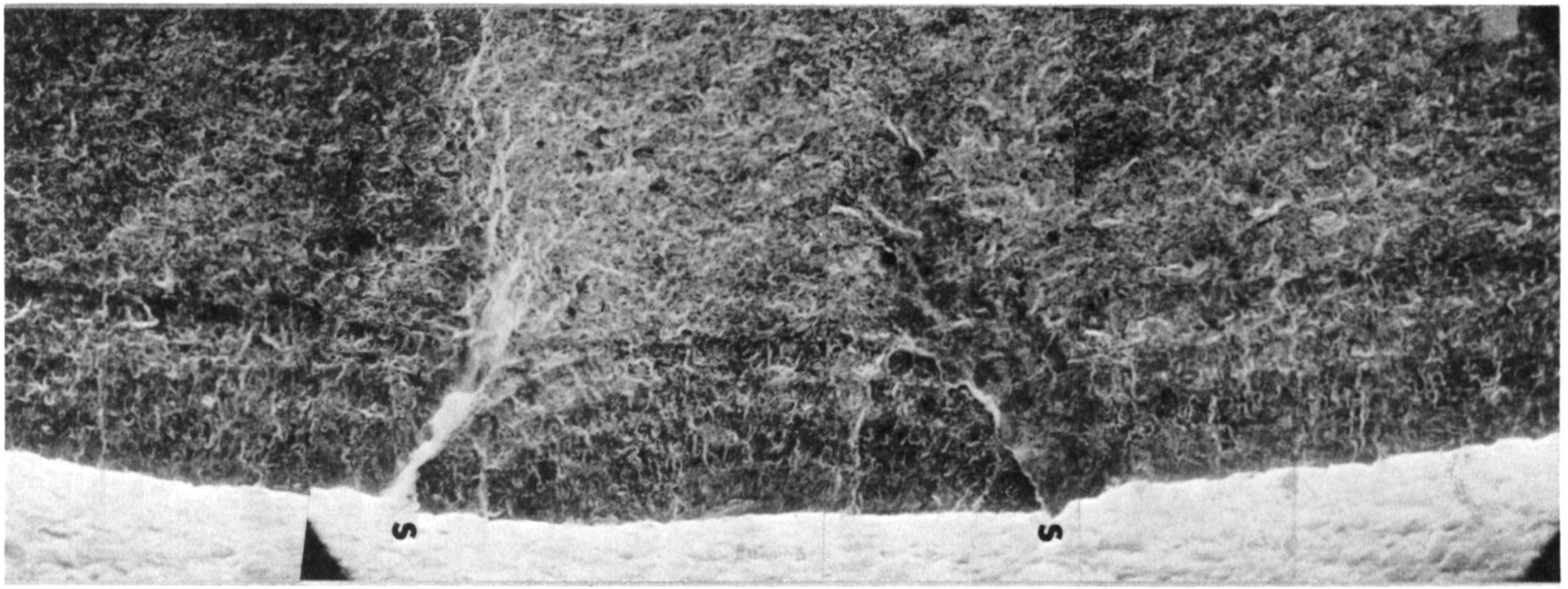

Mag. 27X

Figure 6

Composite of Four SEM Photographs Showing the Suspect Origin Region. The shot-peened surface is on the right side. Stereo-examination revealed that the crescent-shaped region SS was at a lower plane than the rest of the fracture face. The failure was suspected to have originated at the center of SS.

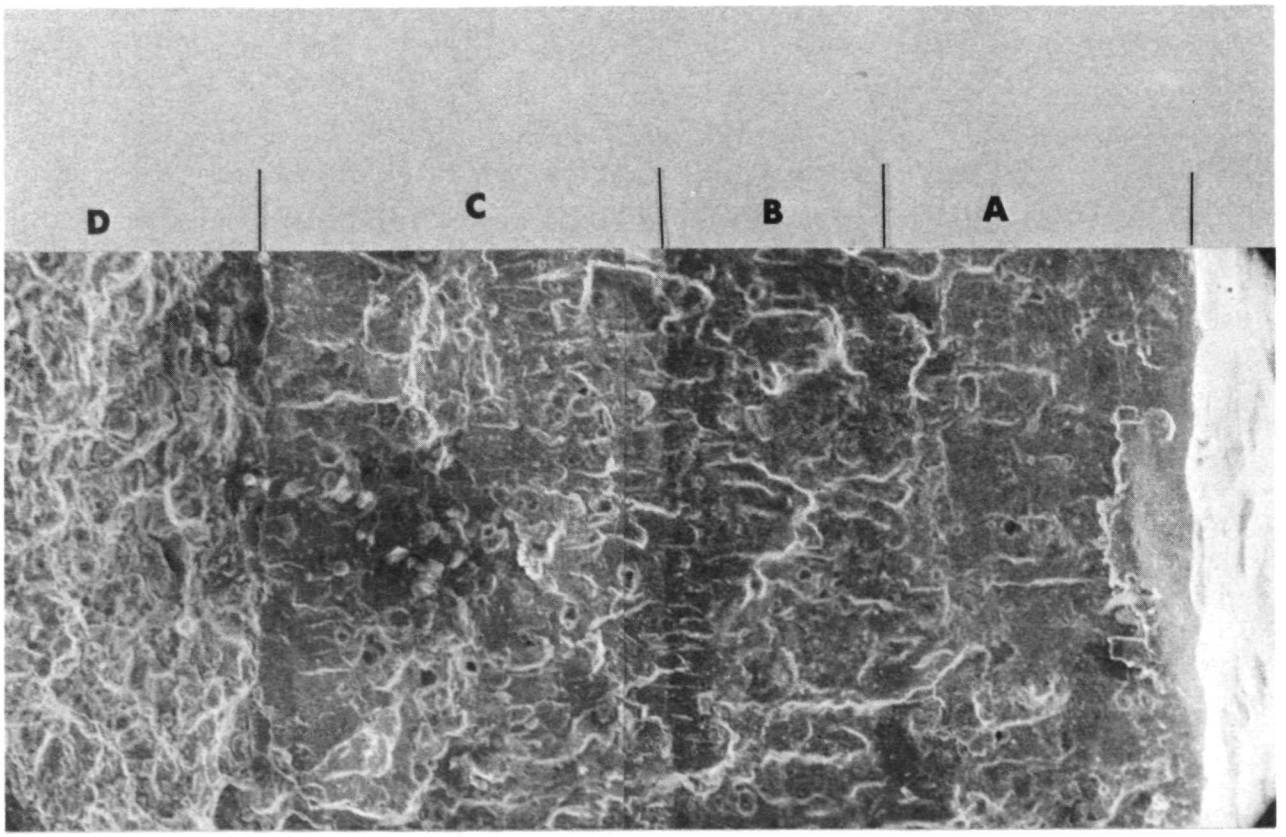

Mag. 140X

Figure 7

Region at the Center of SS in Figure 6, Showing Four Distinct Regions A, B, C, and D.

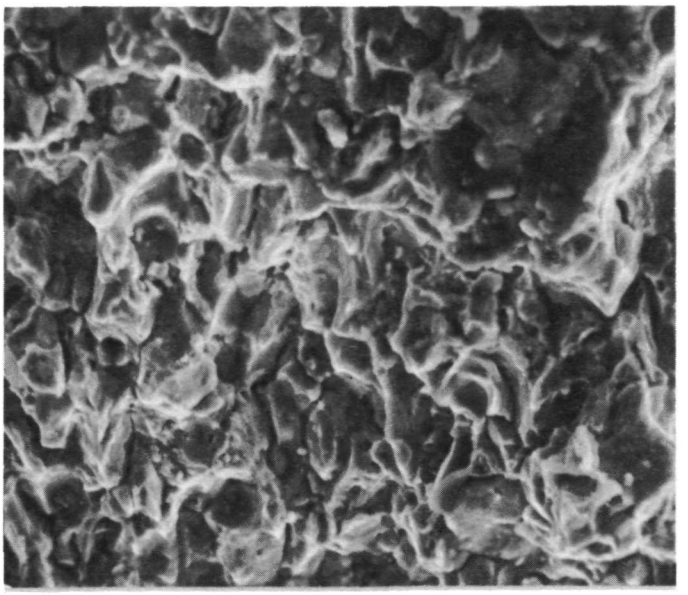

Mag. 300X

(a)

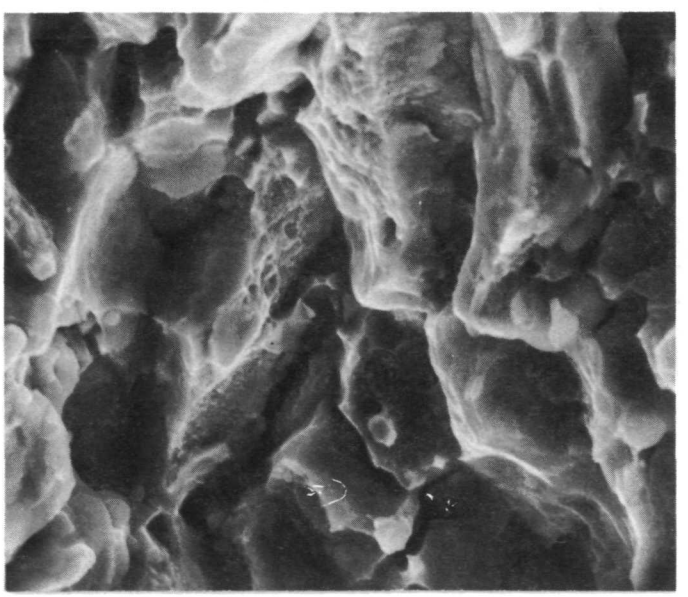

Mag. 1000X

(b)

Figure 8

Typical Features of Region D in Fig. 7
Showing Overload Failure

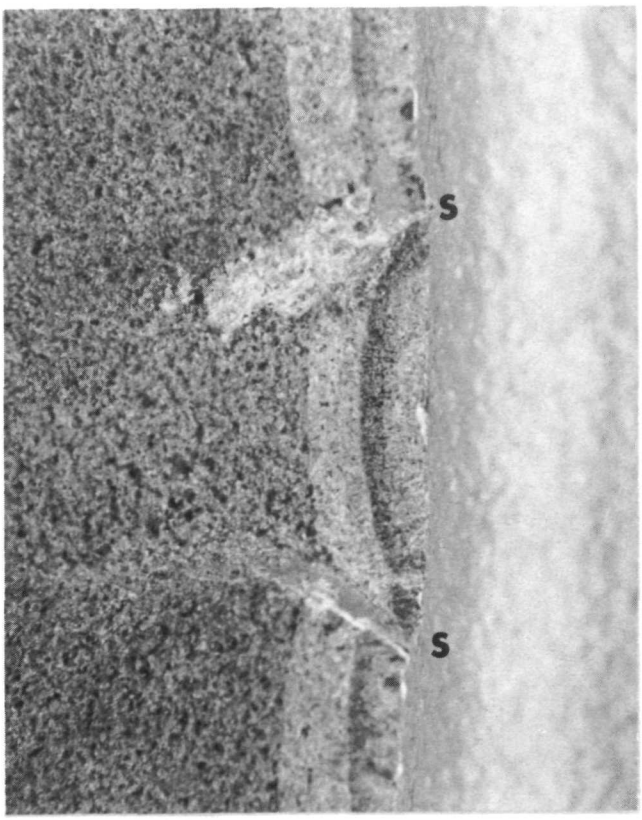

Mag. 18X

Figure 9

Optical Photomacrograph of Suspect Origin in Area 3 (Figure 3).

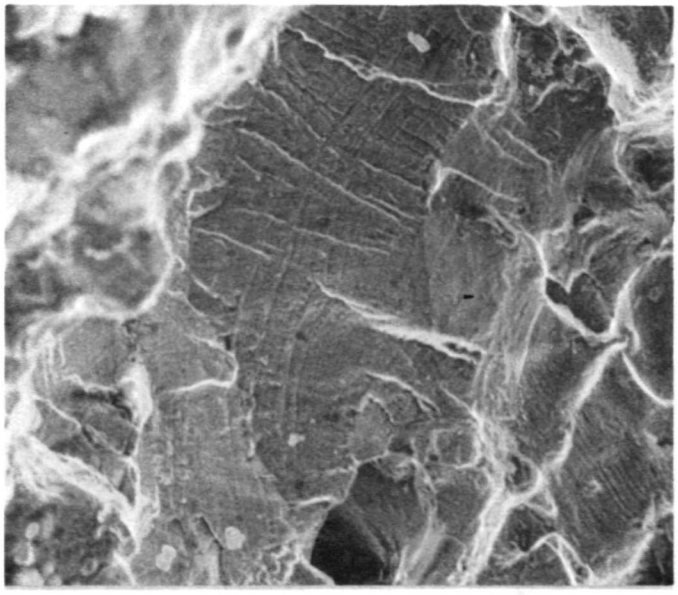

Mag. 810X

(a)

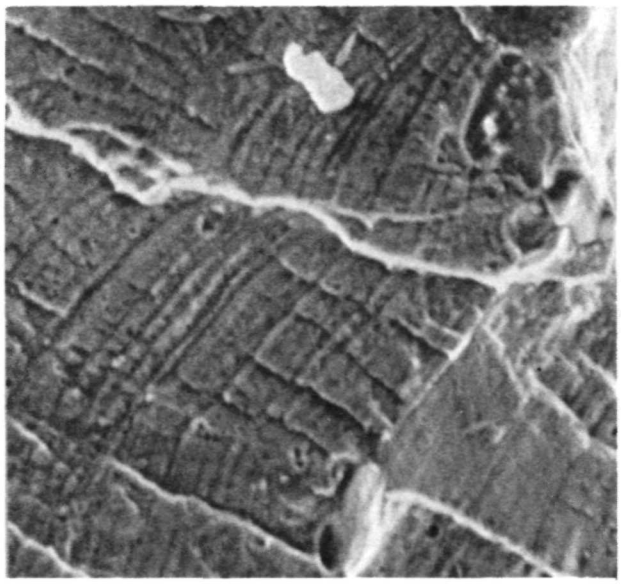

Mag. 2700X

(b)

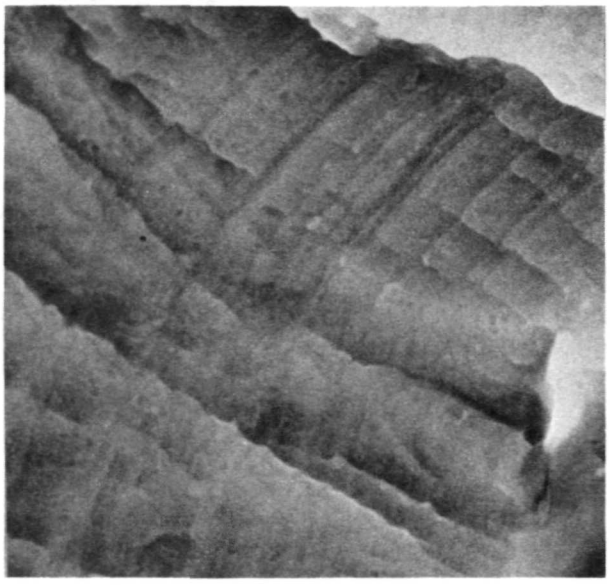

Mag. 3000X

(c)

Figure 10

Fatigue Striations in Region C. (a) Low magnification; while most striations point to the center of SS as origin, local differences in striation direction, attributed to individual grain orientation, are also seen. (b) Higher magnification of the top central region in (a). (c) Another region showing striations in region C. The SEM was operated at 25 kv for this photograph and at 5 kv for the photographs in (a, b); this accounts for the different appearance.

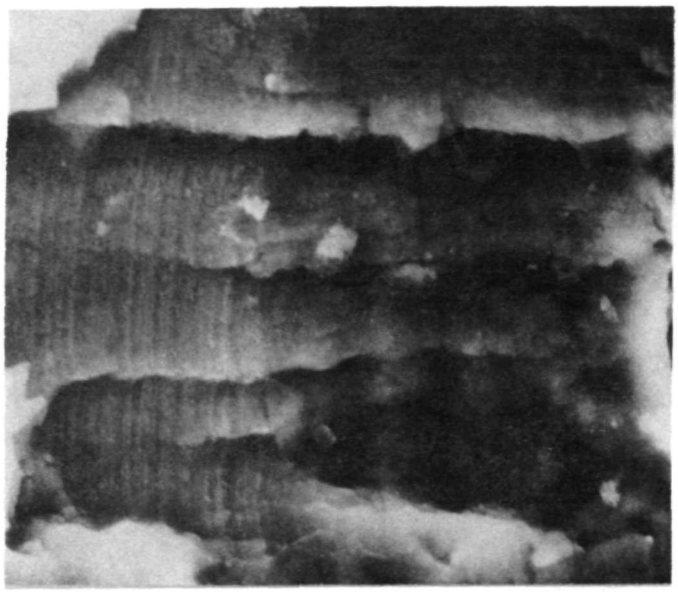

Mag. 500X

(a)

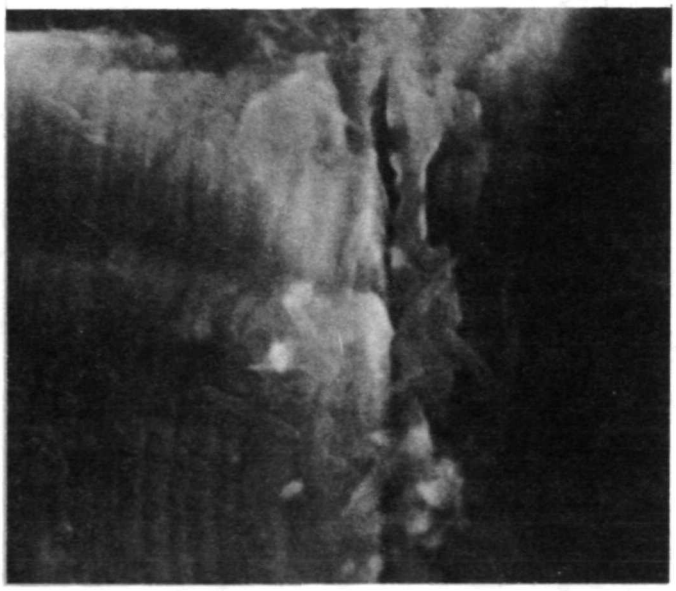

Mag. 6000X

(b)

Figure 11

Region C on the Left and Region B on the Right. The demarcation between the two regions is clearly observed.

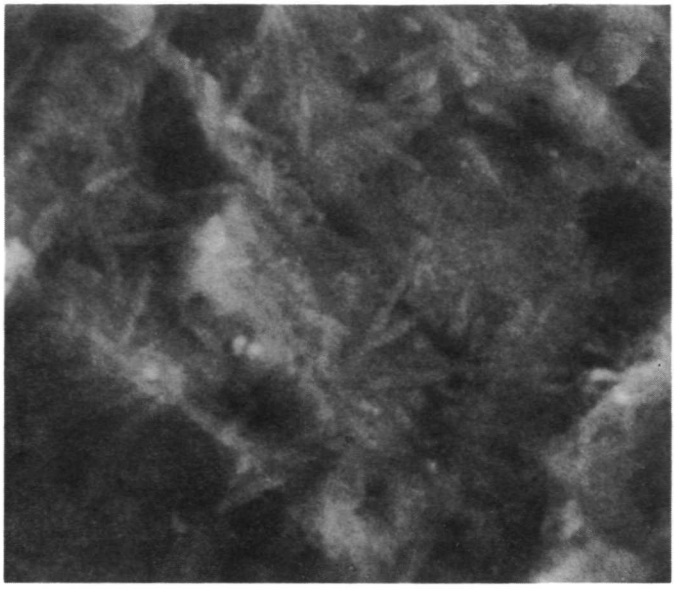

Mag. 7700X

Figure 12

Details of Contaminants Covering Most of the Region B.

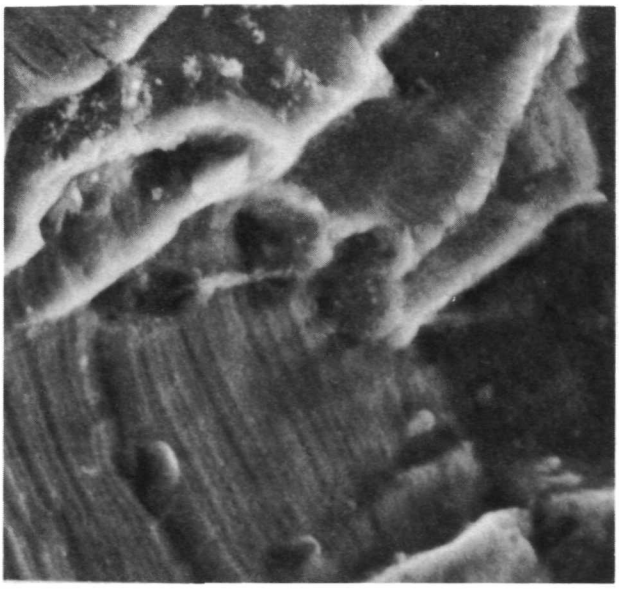

Mag. 2300X

(a)

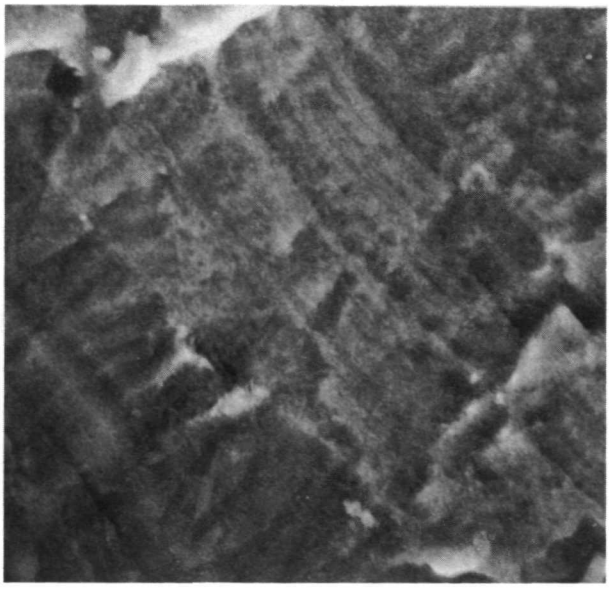

Mag. 2300X

(b)

Figure 13

Fatigue Striations in (a) Region C and (b) Region B. The striations are clearer and sharper in region C than in region B, where they are obscured by contaminants.

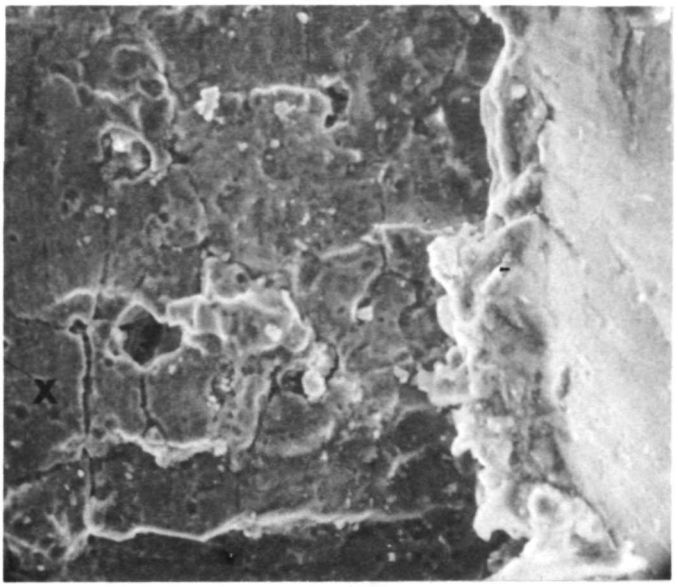

Mag. 460X

Figure 14

High-Magnification View of Region A at the Center of the Fracture Edge in Figure 7.

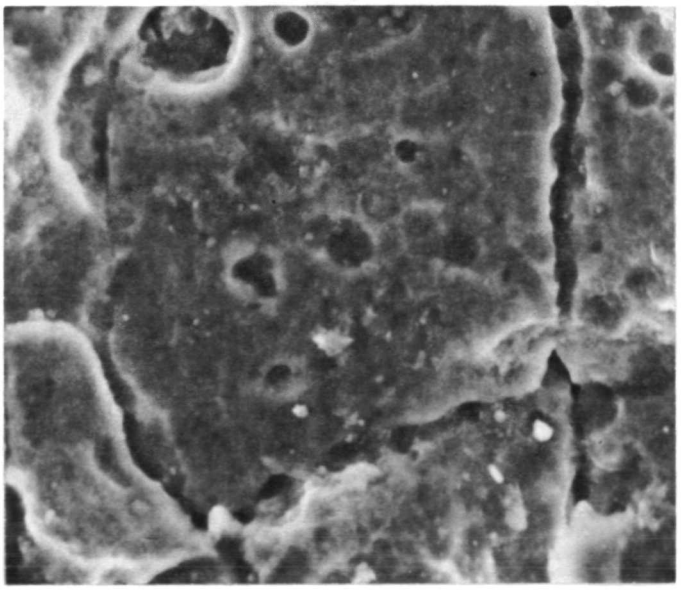

Mag. 1380X

Figure 15

Details of Grain X in Figure 14, Showing Pitting and Grain Boundary Attack.

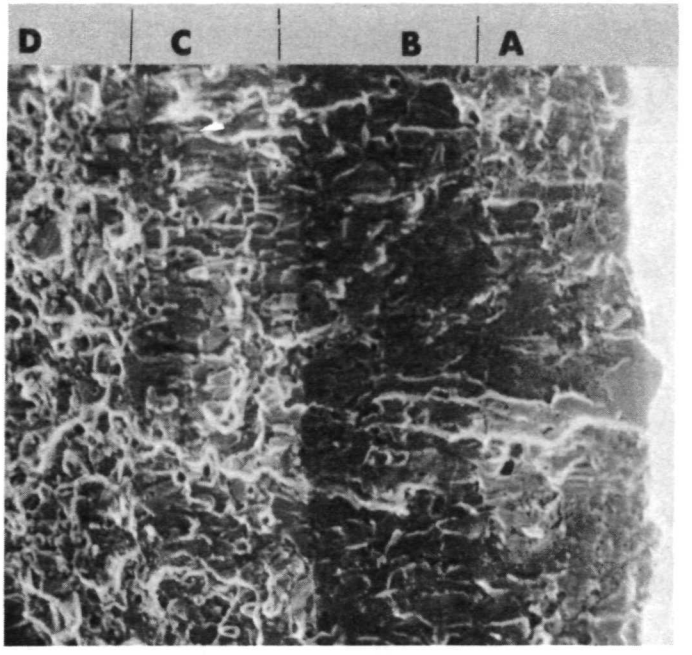

(a) Mag. 100X

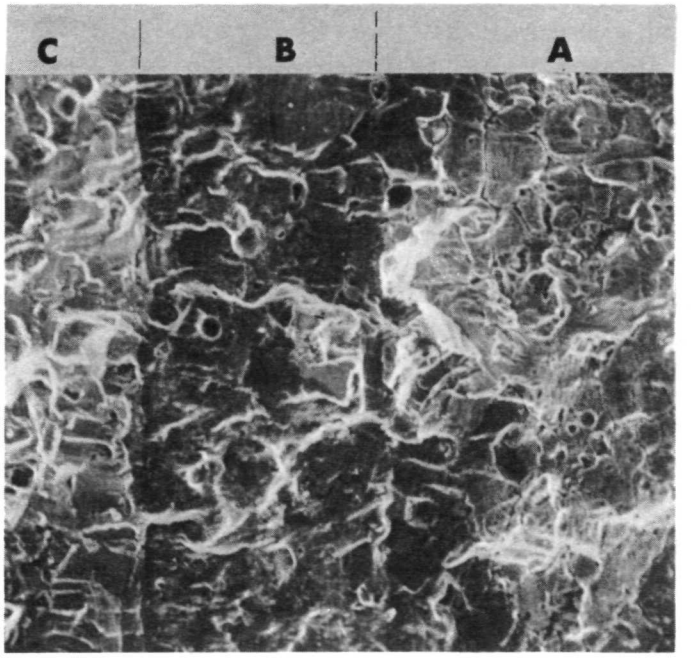

(b) Mag. 230X

Figure 16

Two Areas Outside the Crescent-Shaped Suspect Origin Region SS. Four regions (A, B, C, and D), identical to Figure 7, are observed.

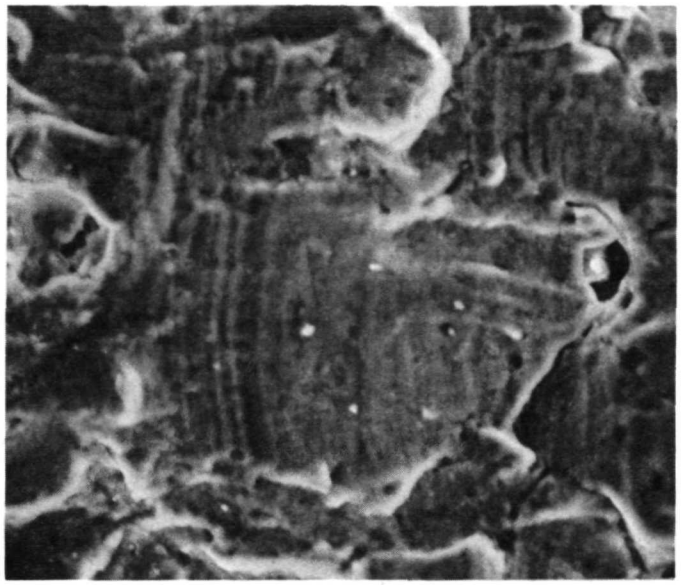

Mag. 770X

(a)

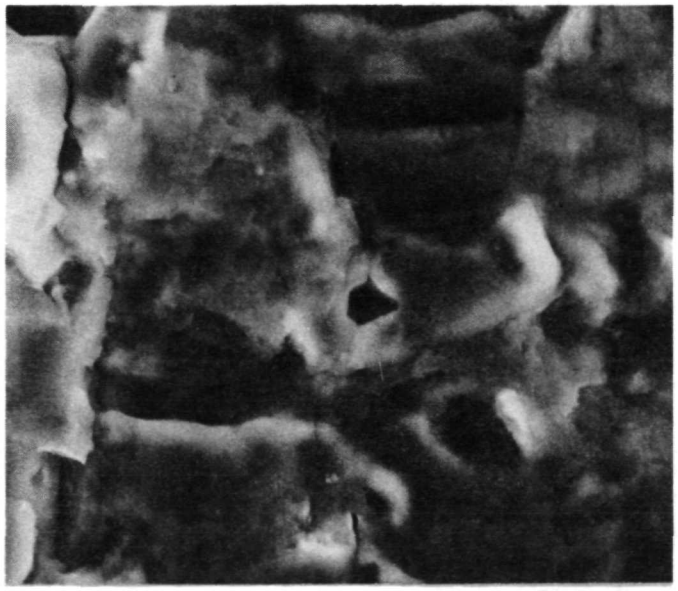

Mag. 1000X

(b)

Figure 17

Two Views of Region B. (a) Presence of fatigue striations is not as clear as in left sides of Figure 18; in (b) fatigue features are not resolved due to surface contaminants.

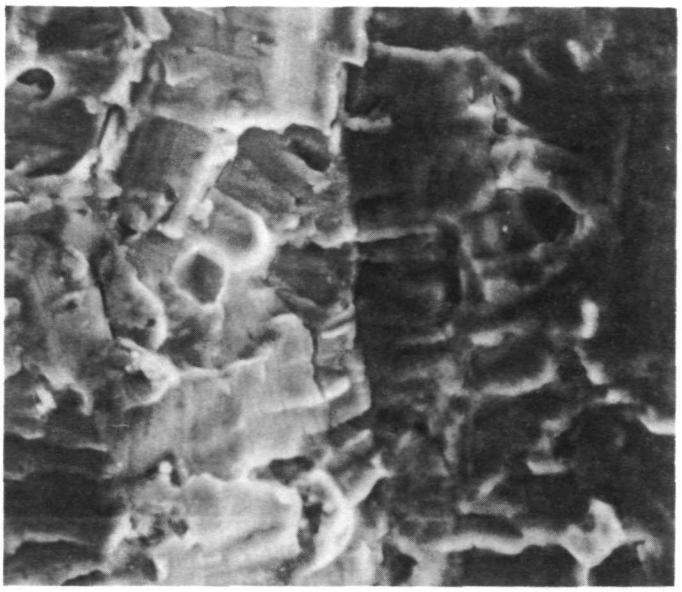

Mag. 500X

(a)

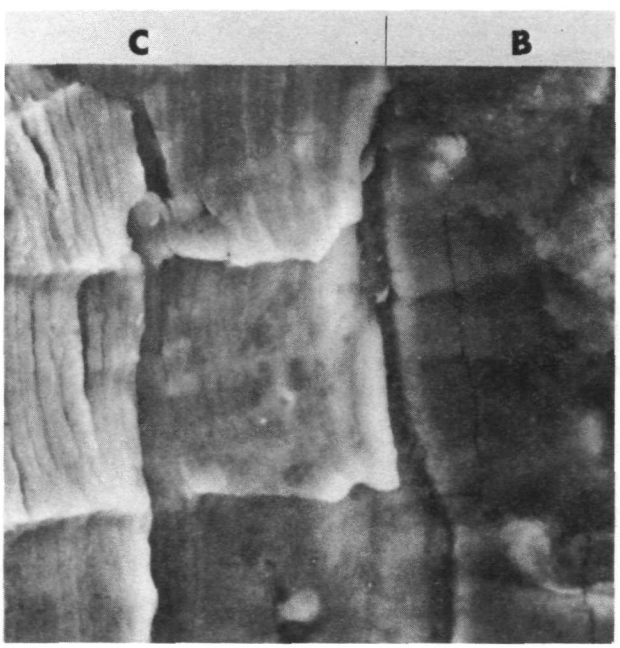

Mag. 2300X

(b)

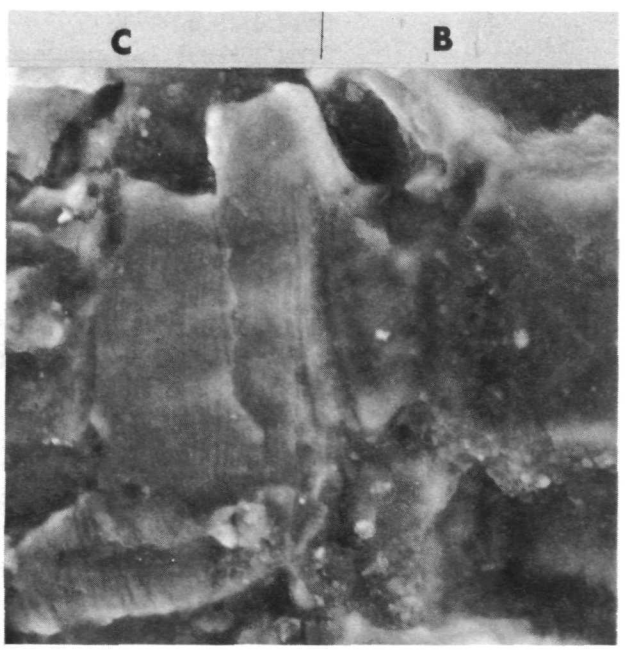

Mag. 1000X

(c)

Figure 18

Views of Regions B and C. (a) Region B on right and region C on left. (b) High-magnification view of center of (a), showing striations in region C and contaminants in region B. (c) Another area showing identical features in regions B and C as in (b).

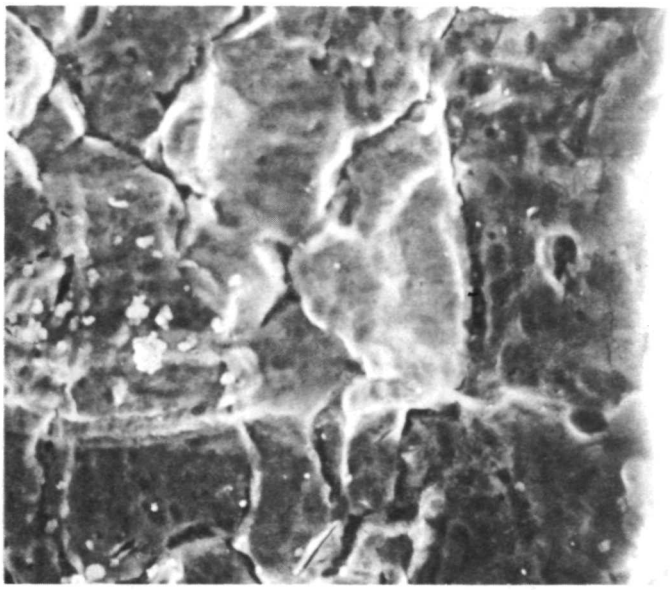

Mag. 770X

(a)

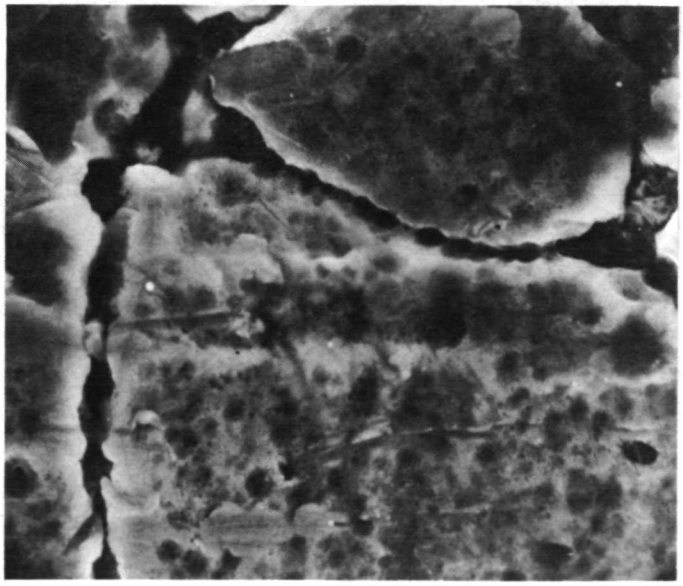

Mag. 2300X

(b)

Figure 19

Appearance of Region A Outside the Crescent Region SS. These features are similar to those of region A in Figures 14 and 15.

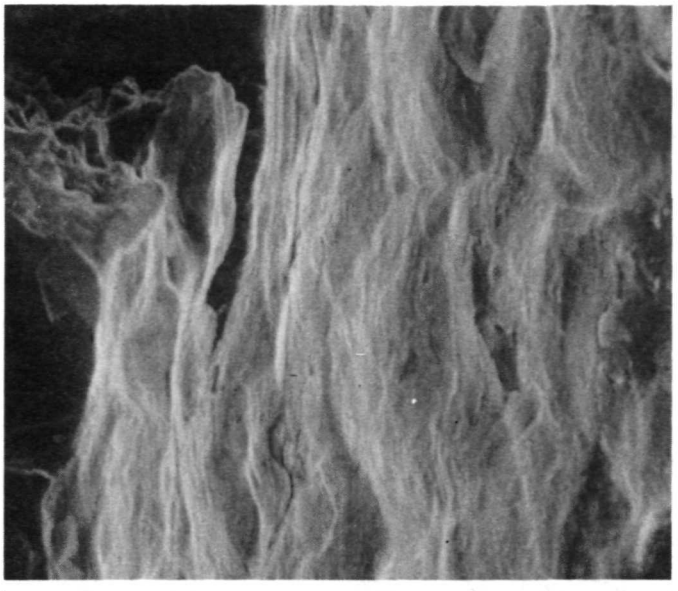

Mag. 180X

(a)

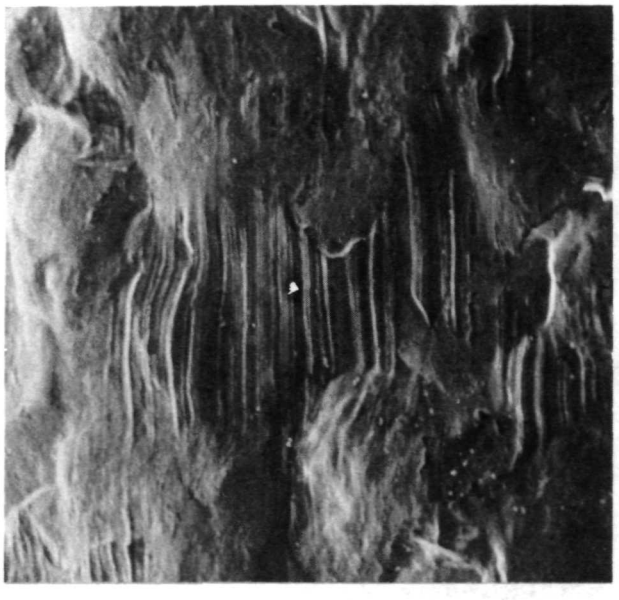

Mag. 180X

(b)

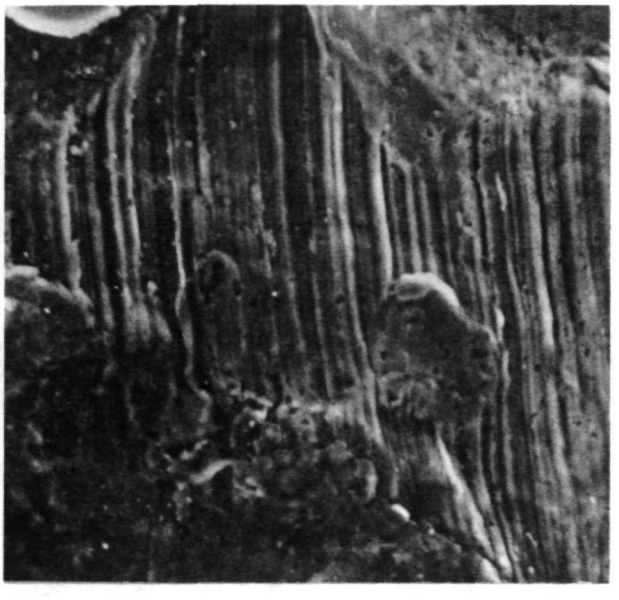

Mag. 500X

(c)

Figure 20

Study of Shot-Peened Surface. (a) Crack on the shot-peened surface at the lower end of the crescent region SS. (b,c) Many areas on shot-peened surface showed presence of original machine markings. Some areas were either unexposed or lightly exposed to the shots, due to poor shot-peening control and hence resulted in local regions of high tensile stresses.

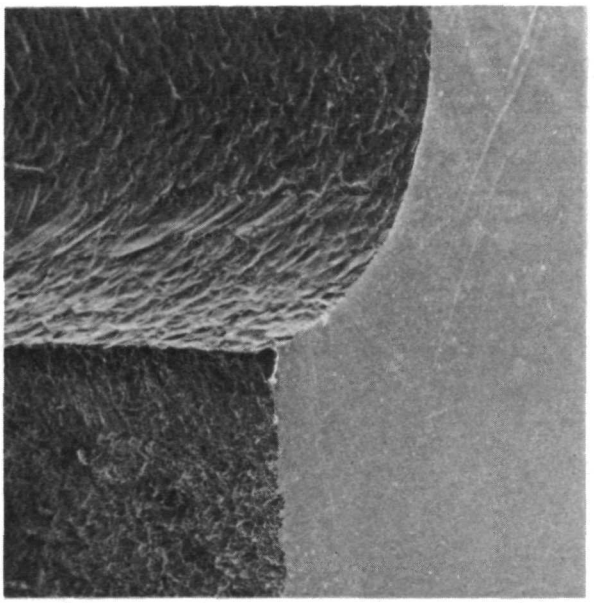

Mag. 24X

Figure 21

Relative Location of Shot-Peened Surface (top left), Fracture Surface (bottom left), and Metallographically Polished Section (right).

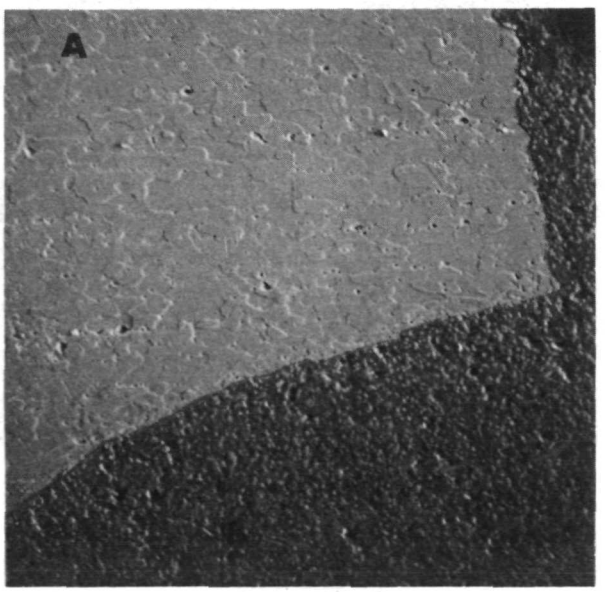

Mag. 100X

Figure 22

Backscattered SEM Photograph of a Section through the Shot-Peened Surface (curved edge) and Fracture Surface (straight edge), Showing the Microstructure of the Alloy (A). Sample is mounted in bakelite (B).

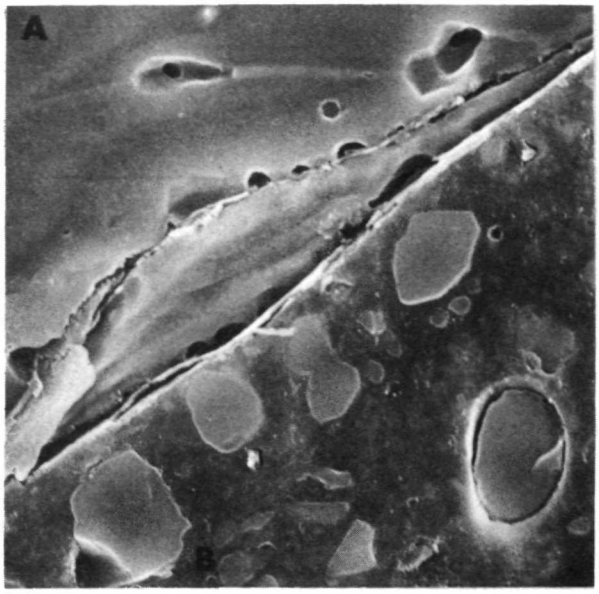

Mag. 2000X

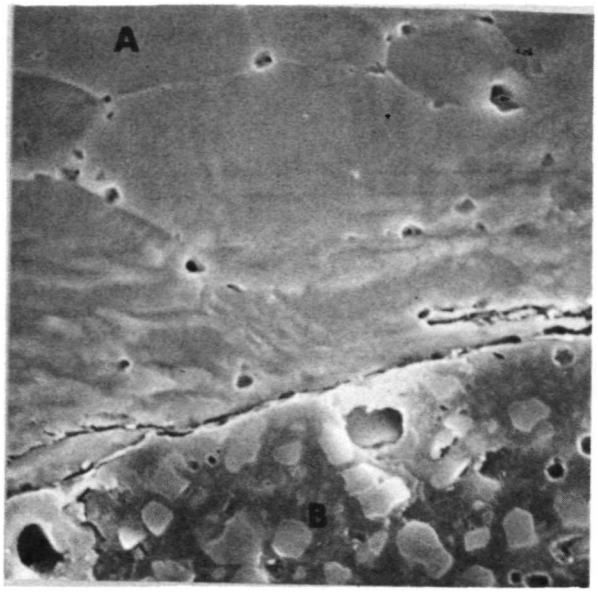

Mag. 1000X

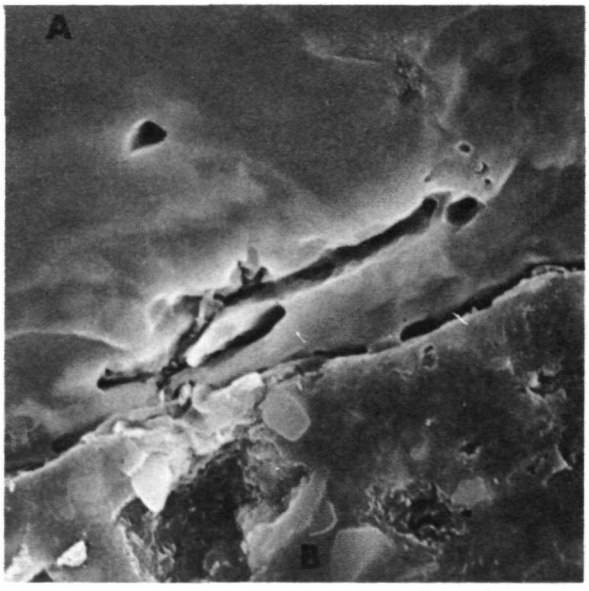

Mag. 2000X

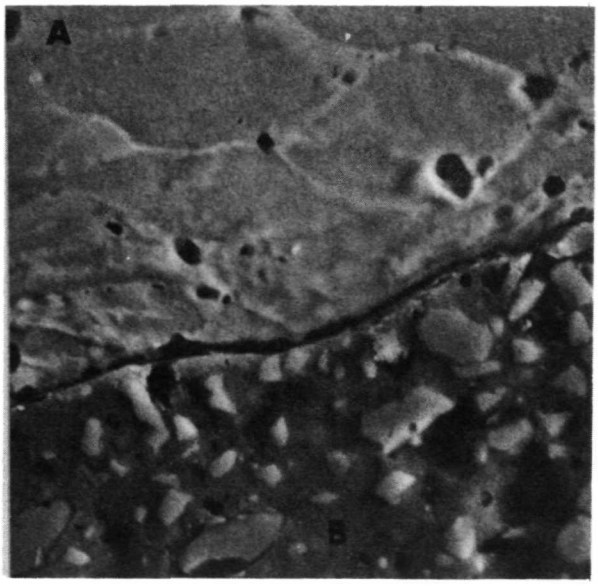

Mag. 1000X

Figure 23

Four Views Showing Details of Shot-Peened Edge in Figure 22. Notice the extent of deformation induced and the nature of defects which are present. (All micrographs are secondary electron images in the SEM.) A is the alloy; B is bakelite.

APPENDIX III

FAILURE ANALYSIS OF ALUMINUM ALLOY COMPONENTS--SAMPLE III

1. INTRODUCTION

This report presents our analysis of failure in a wing spar carry-through forging fabricated from 7075 aluminum. The part was obtained from the Air Force Materials Laboratory. The information supplied with the part indicated that a crack was located near the engine during a routine inspection after 5269 hours of service. The crack had not propagated fully, and the specimen was cut up to open the fracture face. Figure 1 shows an overview of the fracture surface available to IITRI for analysis. It was noted that the edge CC (Fig. 1) had been machined after forging.

2. EXPERIMENTAL

The as-received specimen (Fig. 1) was first directly examined in the SEM. Then the flaw BB was opened up, and exposed surfaces were examined for any clues as to possible defects. Finally, metallographic specimens were prepared and examined for grain flow patterns and cleanliness of the alloy.

3. RESULTS

Fracture surface examined revealed three types of surfaces: The flaw surface, fatigue features originating near the flaw, and a region of overload fracture features. The fatigue surface was present on both sides of the flaw (areas marked A in Fig. 1). The remainder of the fracture surface was overload. The crack did not lead to final fracture because the section size increased after the crack propagated about 10 cm. Only about 2.5 cm of the crack surface (as shown in Fig. 1) was available to us for analysis.

A SEM photograph of the fatigue surface is shown in Fig. 2. The area on the left side of the boundary AA is the flaw surface; the right side is the fatigue surface. Fatigue striations could be readily resolved at all locations in the fatigue region. Two typical areas are presented in Fig. 3. In general, the fatigue striations were parallel to the flaw on both sides of the flaw.

Besides the fatigue region near the flaw, the rest of the fracture surface shown in Fig. 1 was typical of overload failure. A few features are shown in Fig. 4. Dimples, typical of ductile mode of fracture, are present at high magnification, while at low magnifications many particles can be seen, indicating that the alloy in this general area was relatively unclean.

This fact was confirmed during the metallographic examination of a section parallel to the fracture face (Fig. 5). Figure 5a shows the surface near the flaw and machined edge CC of Fig. 1; while the grain flow pattern is good, the machining of the forged surface has rendered the structure weak in the direction perpendicular to the flaw, where fatigue features were observed. Many holes were present on this surface which was prepared by polishing, etching, cleaning with replicas, and coating with gold to prevent charging of bakelite mounting material. Some of these holes lined up along grain boundaries (Fig. 5b), and in some locations inclusions remained intact (Fig. 5c). The chemical analysis of one of these inclusions indicated them to be rich in copper, iron, and aluminum (Fig. 5d); other peaks in Fig. 5d are due to gold from specimen coating.

4. DISCUSSION

The results confirm the conclusion reached by low-power optical microscopy that the mode of fracture was fatigue which initiated at the flaw in the specimen. The large fatigue area on the sample and the close spacings of many striations lead us to conclude that the mode was high cycle fatigue.

The origin of the flaw was considered from many aspects: a flaw resulting from a pipe in the casting and remaining throughout the forging operation; a flaw formed during the forging operation due to improper alignment of dies; or a flaw formed by diffusion of elements during the life of the part. The flaw surface BB (Fig. 1) was opened and examined in detail for any possible clues. No inclusions were found on the surface which appeared oxidized and covered by a surface film (see Fig. 6). The presence of many inclusions in the area close to the flaw (as indicated in Fig. 5)

suggests that the segregation of impurities in the region near the flaw was rather heavy, which would occur if this area solidified last. Hence the cause of the flaw is suggested to be a pipe in the original casting which was forged in and not detected during subsequent nondestructive testing.

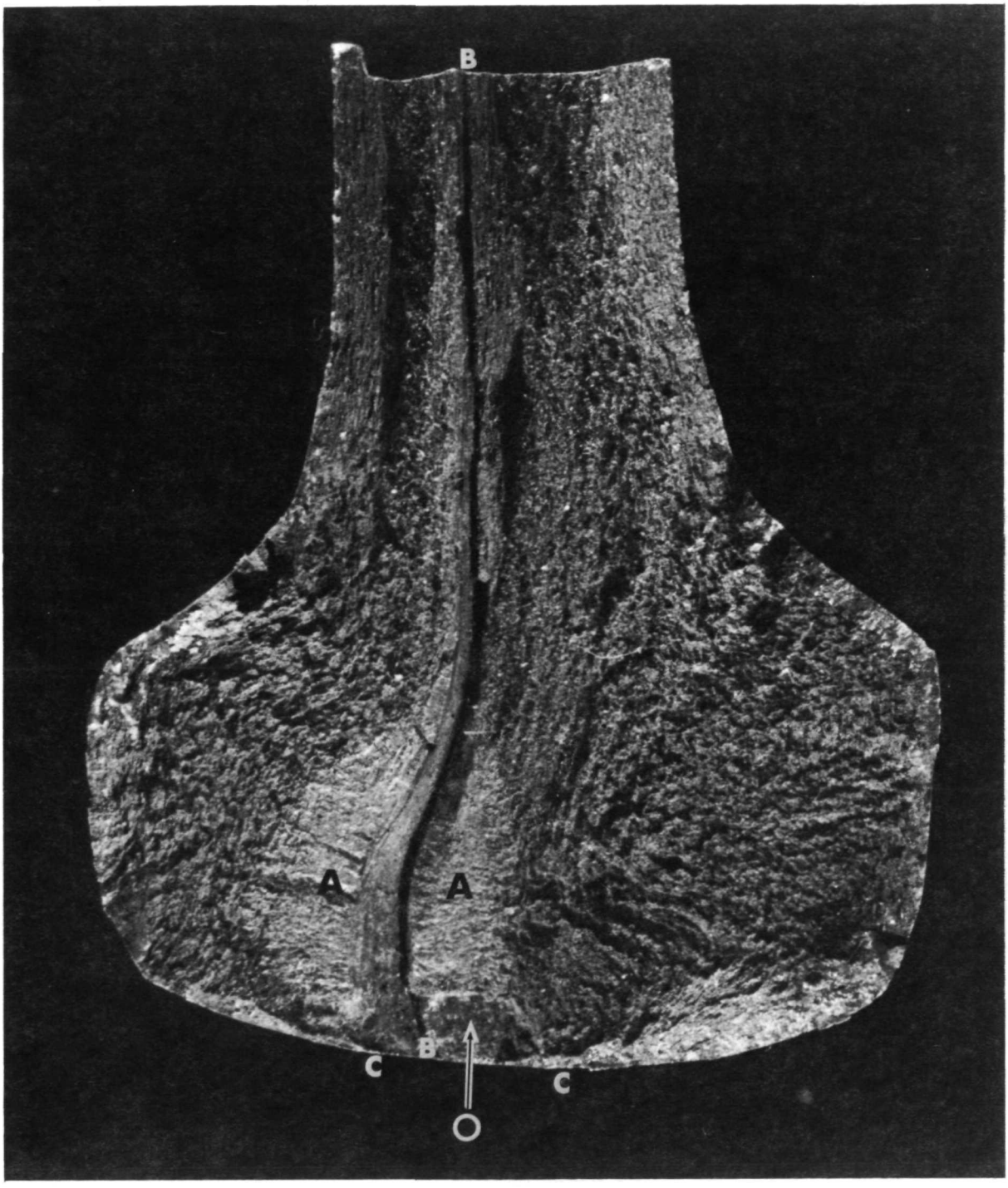

Mag. 5X

Figure 1

Overview of the Fracture Surface of Failed Wing Spar Forging in the As-Received Condition (Optical Photomacrograph)

Mag. 60X

Figure 2

SEM Photograph of Area O in Figure 1. The area right of boundary AA contains many fatigue striations; the area left of boundary is the flaw surface.

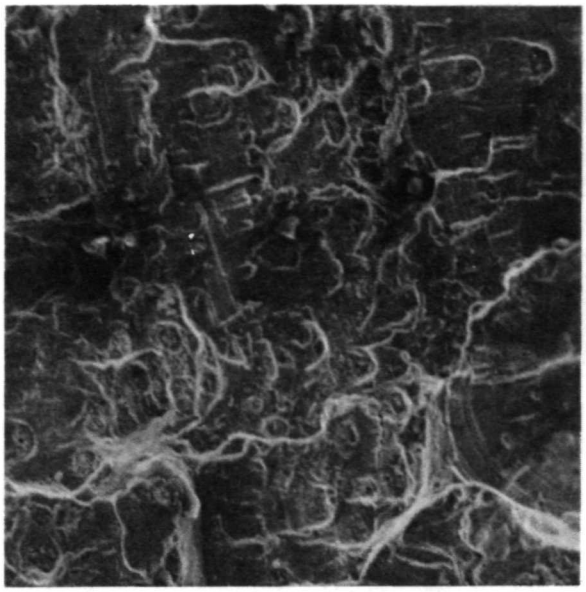

Mag. 300X

(a)

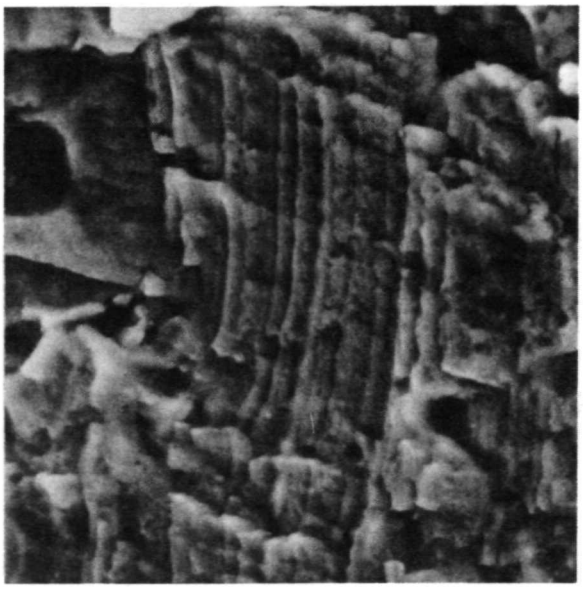

Mag. 2300X

(b)

Figure 3

Fatigue Features--Striations and, in Some Regions, Striations with Dimples. Striations were parallel to the flaw surface.

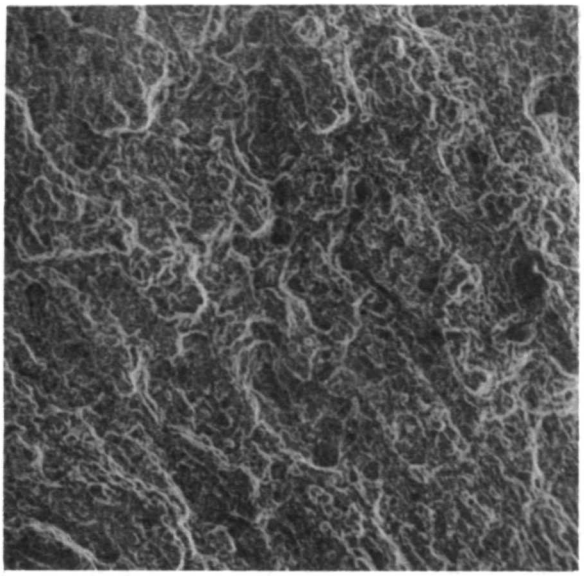

Mag. 60X

(a)

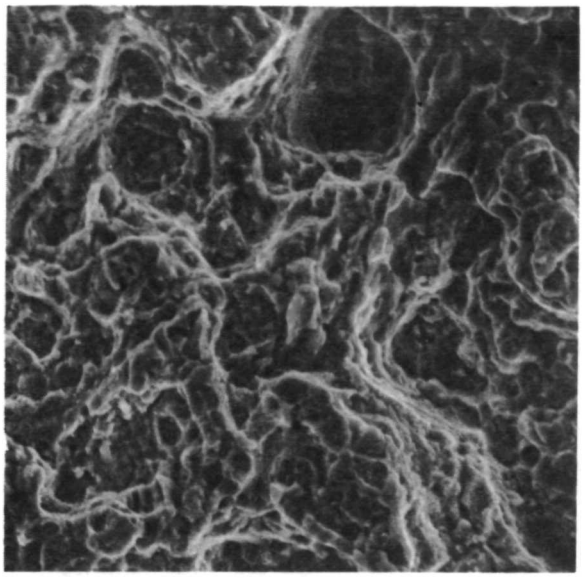

Mag. 300X

(b)

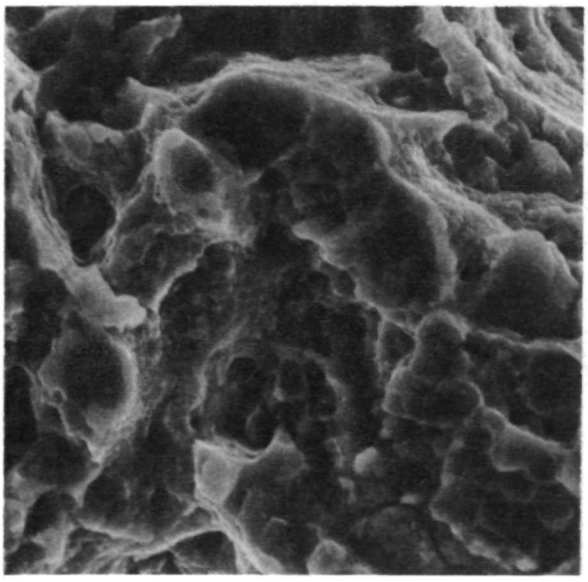

Mag. 1000X

(c)

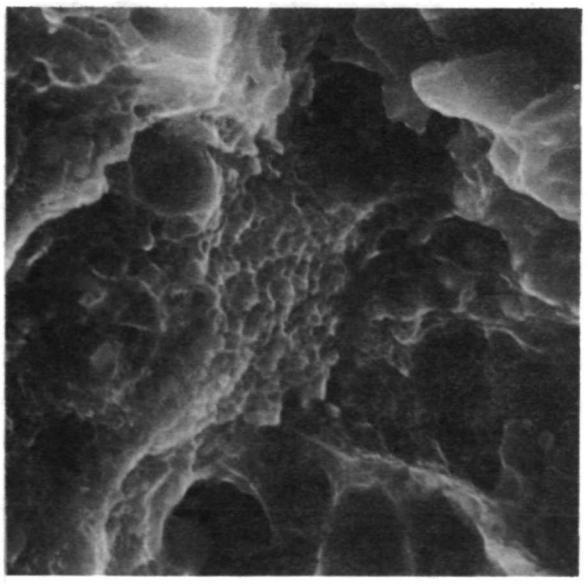

Mag. 3000X

(d)

Figure 4

Overload Features at a Range of Magnifications. The center area of the low-magnification photograph (a) is progressively magnified in (b), (c), and (d).

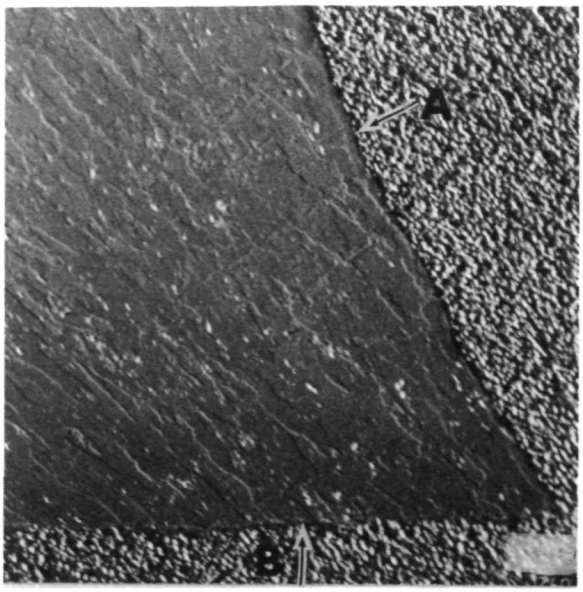

Mag. 60X

(a)

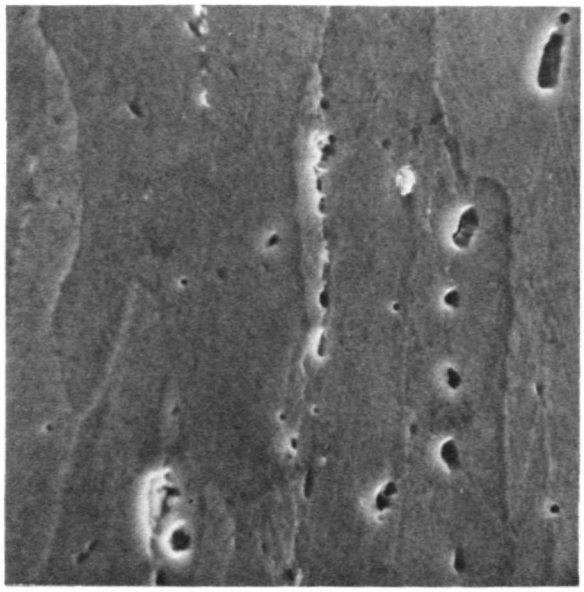

Mag. 1000X

(b)

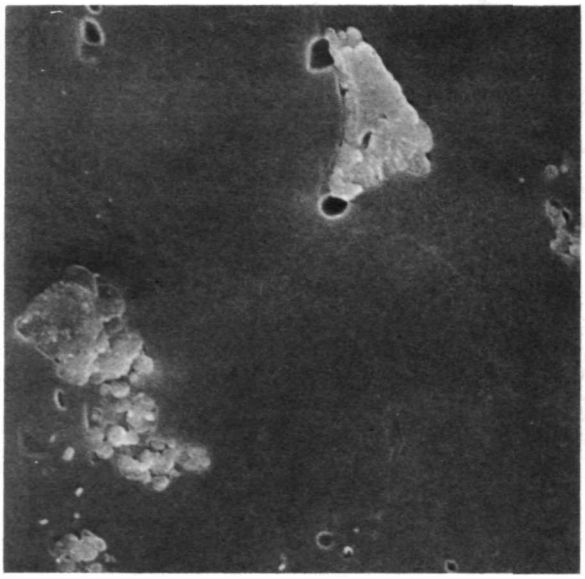

Mag. 1800X

(c)

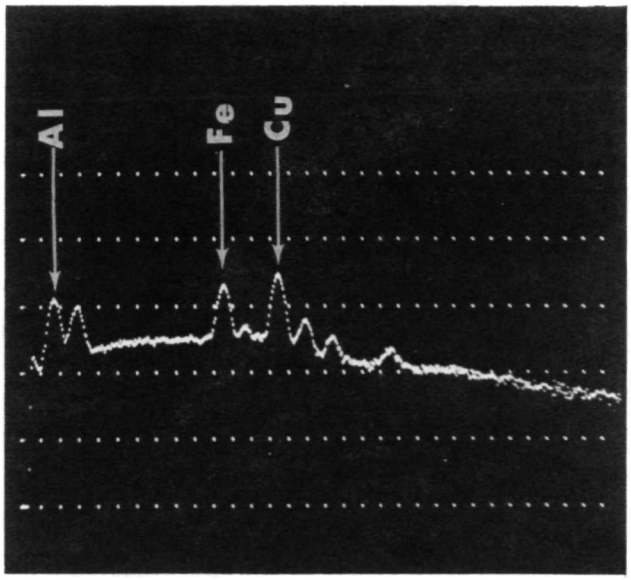

X-ray

(d)

Figure 5

SEM Metallographic Study--(a) overall view, A is the flaw surface; B the machined top surface; (b) details of some holes along grain boundaries indicating segregation; (c) some areas showed inclusions whose analysis in (d) indicated them to be iron and copper rich.

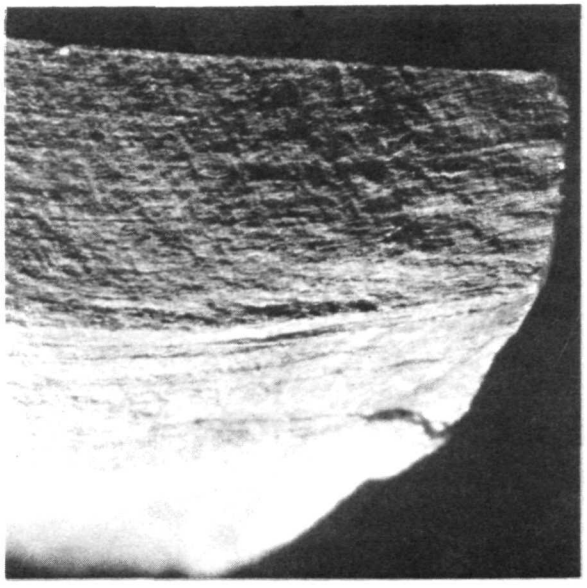

Mag. 15X

(a)

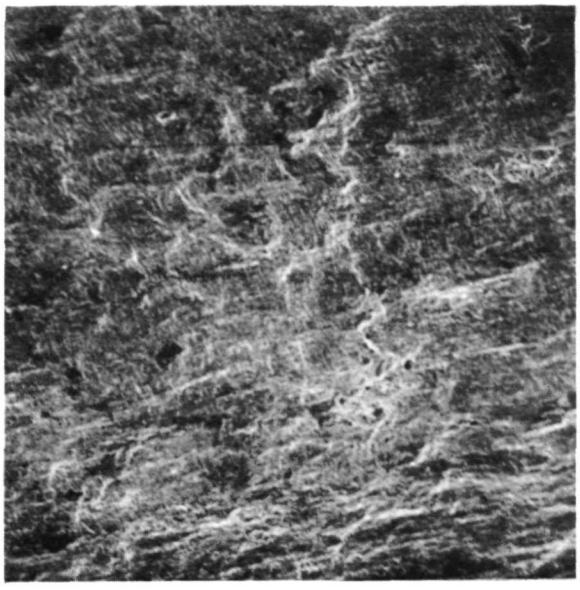

Mag. 45X

(b)

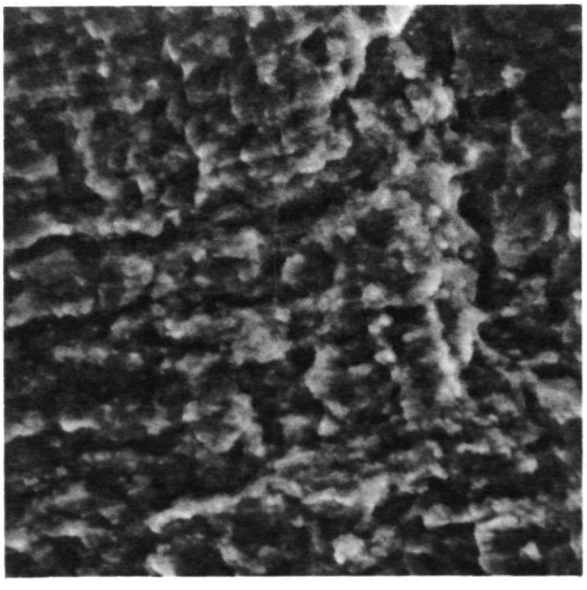

Mag. 450X

(c)

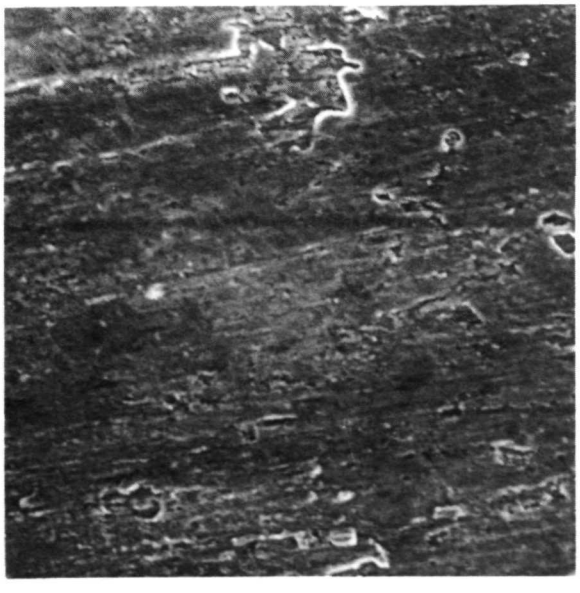

Mag. 135X

(d)

Figure 6

Four Views of the Surface of the Flaw: (a) Optical and (b) SEM photograph of an area near the machined top edge CC in Figure 1; (c) center area of (b); (d) an area away from the machined edge.

APPENDIX IV

FAILURE ANALYSIS OF ALUMINUM ALLOY COMPONENTS--SAMPLE IV

1. INTRODUCTION

This report presents the analysis of failure in a rear horizontal elevator recovered from an aircraft crash. Although many broken components were obtained and examined by the Air Force Materials Laboratory, IITRI had access only to the bell crank fitting, the fracture surface of which is presented in Fig. 1. The material for the component was aluminum alloy 356 in the as-cast and T6 condition. On visual examination no initiation point of the fracture could be located.

2. EXPERIMENTAL METHOD

The as-received specimen was examined with a low-power binocular microscope. Initial SEM examination revealed that the specimen was dirty and, accordingly, it was cleaned in the ultrasonic cleaner with trichloroethylene.

3. RESULTS AND DISCUSSION

The features on the fracture surface of this part were uniform over the whole surface. Figure 2 is a low-magnification photograph. Many areas containing undisturbed features are evident. A high-magnification examination (Fig. 3) revealed that these features are associated with the porous regions of the casting. Some porosity is normally expected in every casting, and a propagating crack will go through the pores if they lie close to the crack plane.

Examination of the rest of the sample revealed that fracture features were typically alike. Four views of these are presented in Fig. 4. These features are associated with the solidification and heat-treated structure of the casting. A comparison of these micrographs was made with the tensile overload and impact fractures in aluminum 356 castings from the fractography handbook.[2] The presence of dimples in many areas was noted in

both handbook samples, but no dimples were observed in the failed sample. Although the material was the same, the handbook samples were in the as-cast condition while the failed part was in the T6 condition. This difference in material condition could account for the difference in fractographic features between the two and hence prevented direct comparison.

Miniature impact and tensile samples were prepared from other areas of the supplied failure and examined in the SEM. In all samples (the failure, the two handbook examples, and the miniature tensile and impact samples made from areas slightly away from the fracture face of the failure) the features associated with porosity (as presented in Fig. 3) were readily observed, and a comparison to determine the mode of fracture could not be made based on these features alone.

Figure 5 presents some of the general features of the miniature tensile specimen, and Fig. 6 shows the miniature impact sample. The presence of dimples in many areas of the sample in Fig. 5 and their absence on the fracture face of the failure clearly rule out that the failure was due to overload. The similarity between the miniature impact sample and the failure sample is striking, and the obvious conclusion is that failure in this part was caused by impact.

Since the part was obtained from a plane crash, impact-caused failures are a distinct possibility. The casting does have a very poor impact strength (one sample tested in the as-cast condition for the handbook had a Charpy impact strength of only 3 ft/lb, and this value should be further reduced in the heat-treated T6 condition). Our results only show that, in this particular part, the fracture was caused by impact, regardless of what the fracture modes were in other components.

The reasons for the absence of dimples and the presence of the same features as observed in the impact fractures (Figs. 4 and 6) were sought by examining the microstructure in this alloy. Figure 7 shows some of the features observed in the secondary

mode on an unetched surface. As expected, a heat-treated eutectic structure is observed; the dark areas in Fig. 7d are rich in silicon. The white streaks are presumably inhomogeneous inclusions because X-ray analysis shows them to be rich in aluminum and iron. The fracture surface observed corresponds to this microstructure by showing crack propagation through the eutectic regions, porosity, inclusions, and grain boundaries. Hence, very little ductility is observed.

4. CONCLUSIONS

In addition to establishing that the part failed by impact (and this conclusion could only be arrived at by use of the SEM capability), this failure analysis indicates the following significant conclusions:

1. The handbook-type approach--i.e., comparing fracture features of laboratory-generated failures with service failures--is extremely valuable. However, care must be taken that the material selected is comparable in both cases. This is more critical in cast structures, where the microstructure varies widely as a function of casting parameters (mold type, thickness, cooling rate, location of the region, and segregation).

2. A comparison of the fracture features (Figs. 3, 4, 5, and 6) with microstructure (Fig. 7) illustrates that, from a property-structure correlation standpoint, considerably more information is obtained from the fracture surface examination than from the polished and etched section. This was predicted over 50 years ago,[5] but the SEM enables this approach to become a reality.

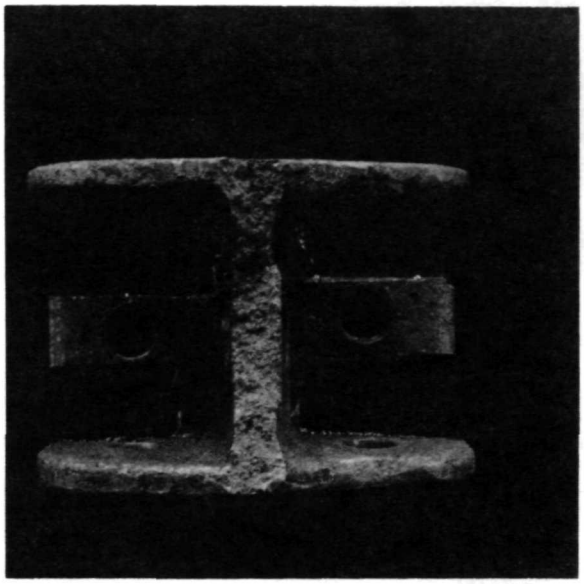

Mag. 1.5X

Figure 1

Optical Photomacrograph of Fracture in Bell Crank Fitting of Horizontal Elevator in As-Received Condition.

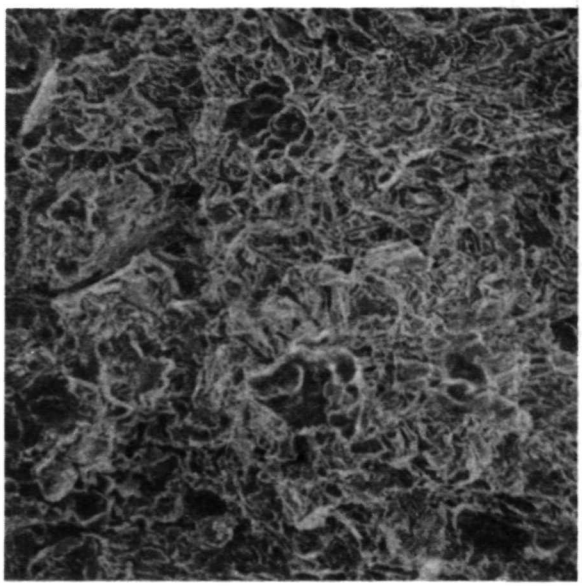

Mag. 60X

Figure 2

A Typical Area at Low Magnification.

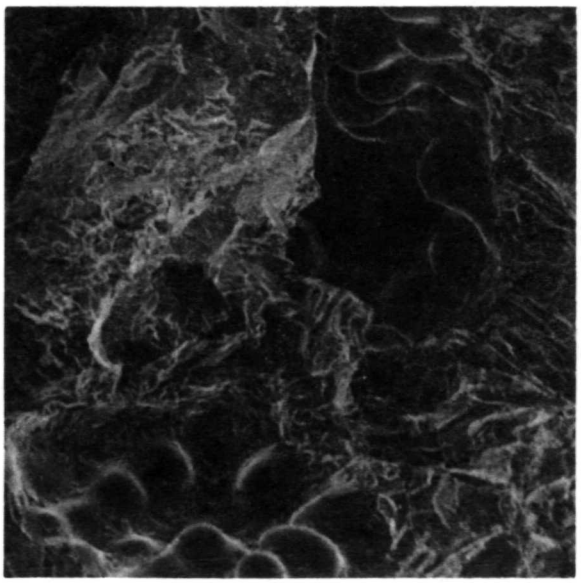

Mag. 270X

Figure 3

Fracture Surface Features That Are Associated with Porous Regions.

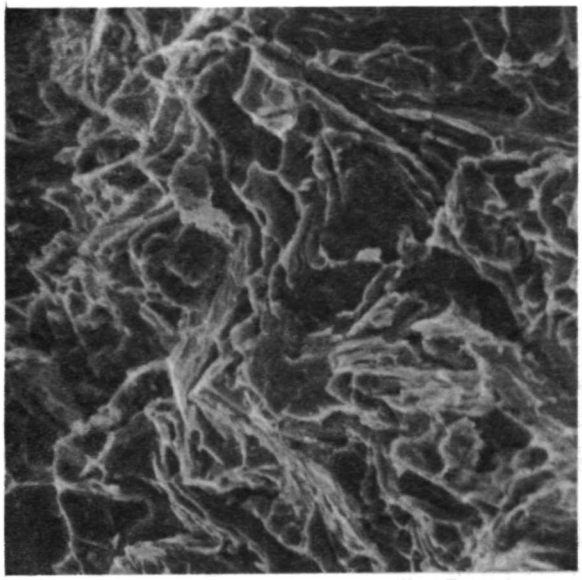

Mag. 300X

(a)

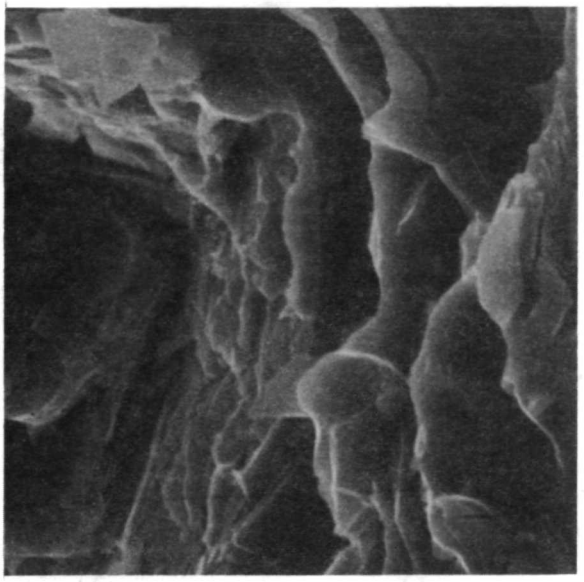

Mag. 1500X

(b)

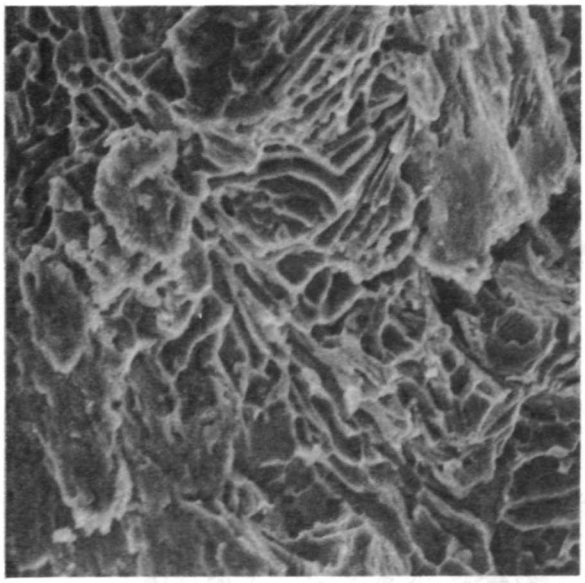

Mag. 300X

(c)

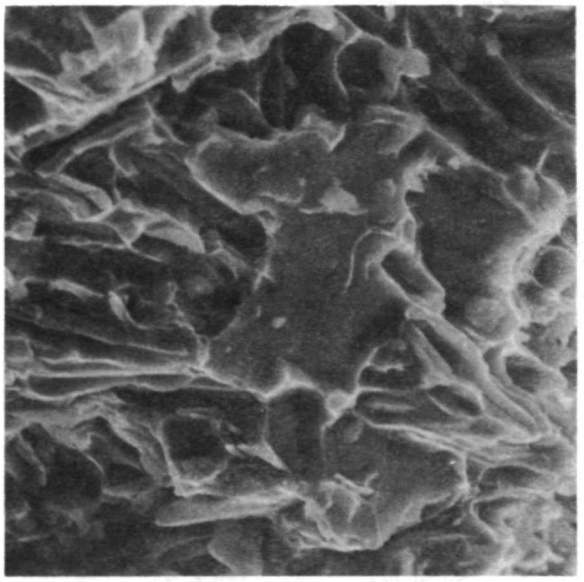

Mag. 1000X

(d)

Figure 4

Typical Fracture Features. (a) and (b) are for the same area; (c) and (d) are for two other areas.

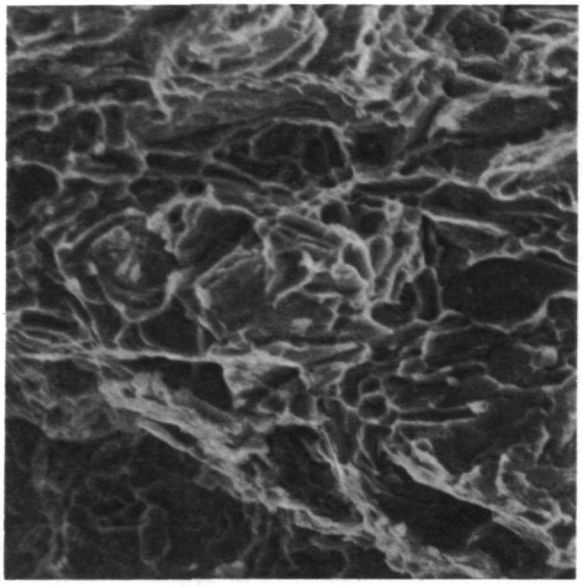

Mag. 300X

(a)

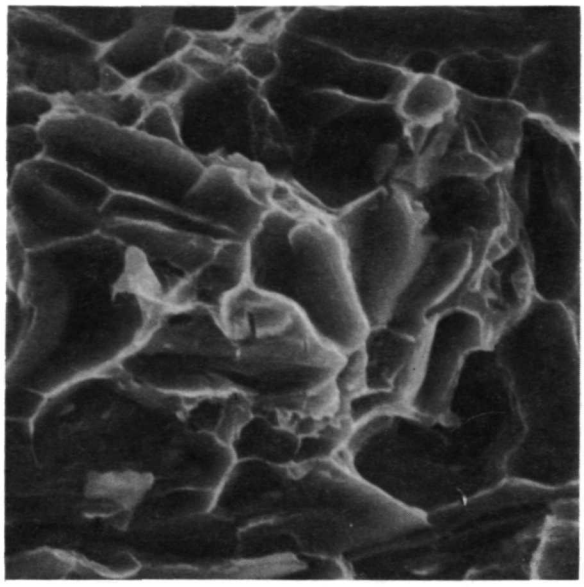

Mag. 1000X

(b)

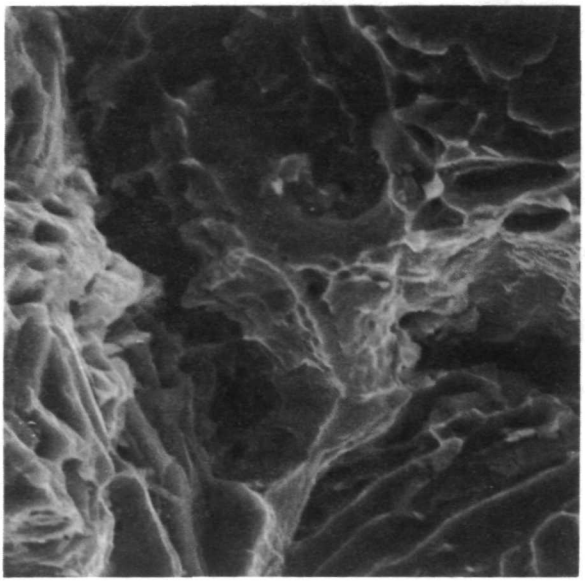

Mag. 300X

(c)

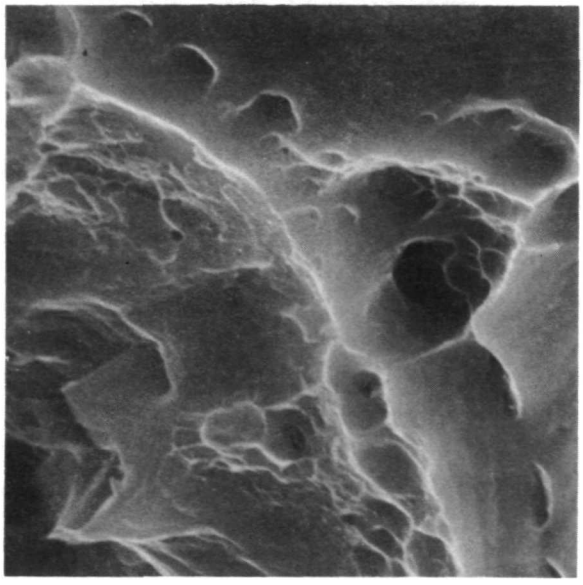

Mag. 3000X

(d)

Figure 5

Four Views of Fracture Features in the Miniature Tensile Sample Made from a Piece of the Specimen in Figure 1.

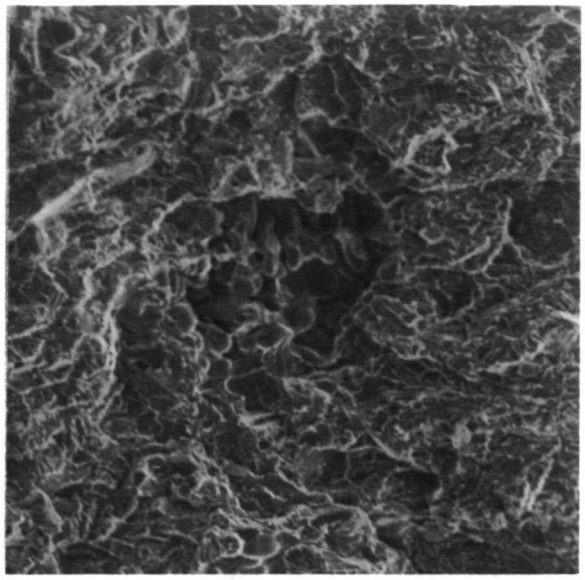

Mag. 60X

(a)

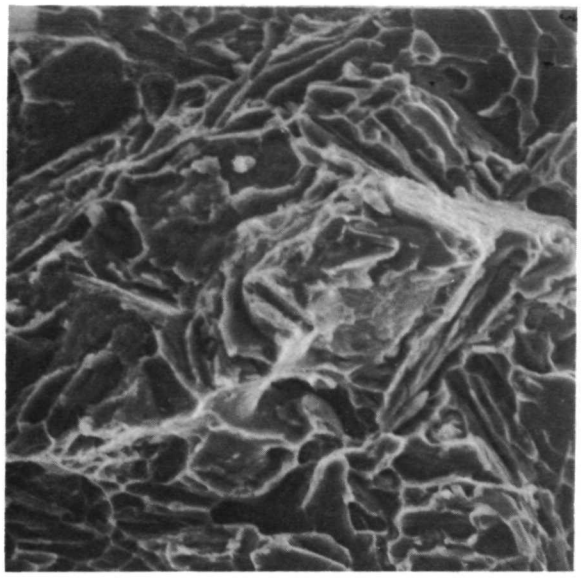

Mag. 300X

(b)

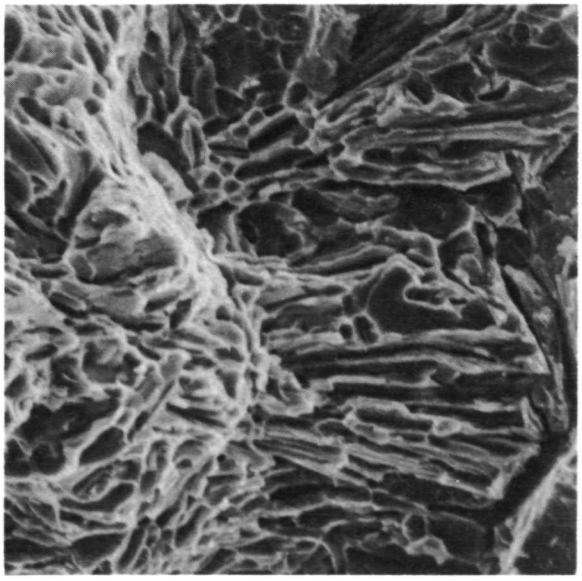

Mag. 300X

(c)

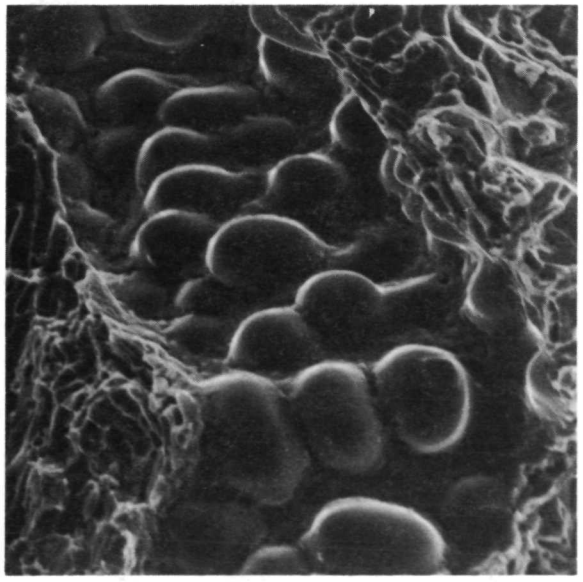

Mag. 270X

(d)

Figure 6

Four Views of Fracture Features in the Miniature Impact Sample Made from a Piece of the Specimen in Figure 1.

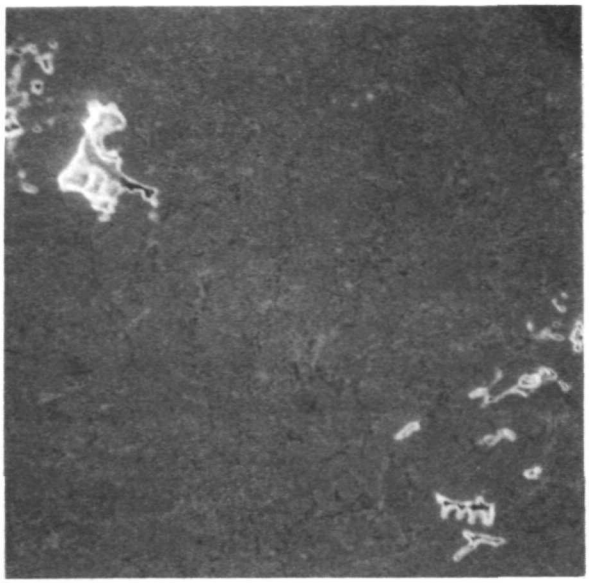

Mag. 60X

(a)

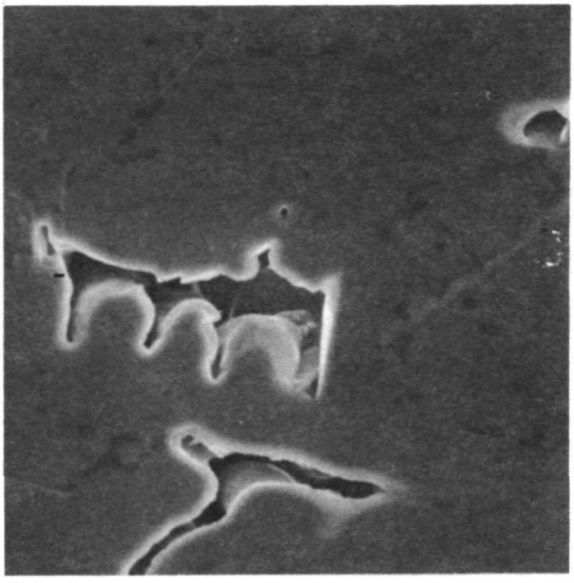

Mag. 300X

(b)

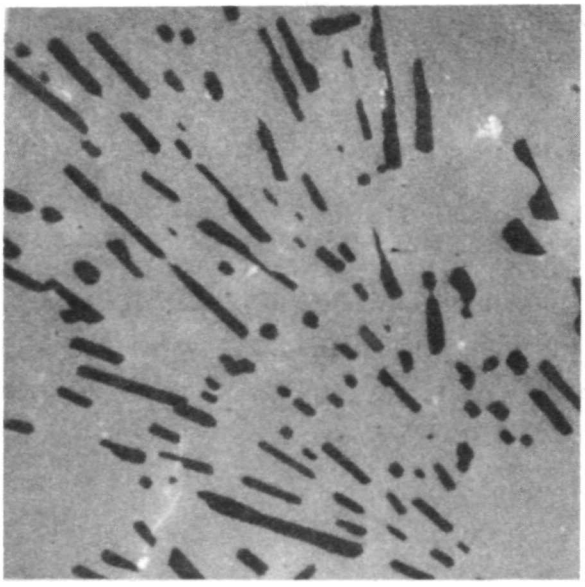

Mag. 200X

(c)

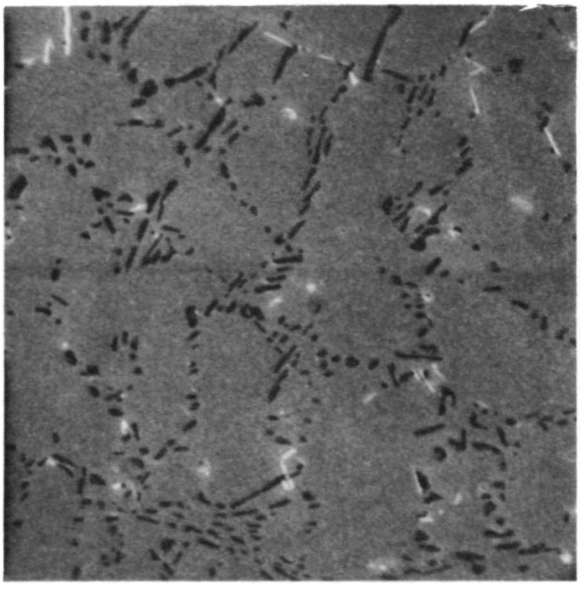

Mag. 600X

(d)

Figure 7

SEM Photographs of a Polished and Unetched Section, Showing Porosity and Heat Treated Eutectic Structure.

APPENDIX V

FAILURE ANALYSIS OF ALUMINUM ALLOY COMPONENTS--SAMPLE V

1. INTRODUCTION

This report presents our analysis of a failure in a bomb rack side plate. The plate was made from 7075 aluminum alloy in the T-6 condition. The part was obtained from the Air Force Materials Laboratory. The following background information was obtained from AFML. The bomb rack side plates were used in conjunction with a ground test facility for testing fuel tanks, by helping support the fuel tank in a 25 hr qualification test. The rigorous tank qualification test subjected the system to a corrosive environment under spectrum loading. The fatigue cracking was observed to initiate from the attachment hole at the end of the rack.

2. EXPERIMENTAL

Figure 1 presents the fracture face in the condition received by IITRI. The crack had already been opened up by sawing the piece (saw marks are visible at left in Fig. 1). Some corrosion product is visible near the hole, this area is magnified in Fig. 2. A 2.5 cm piece was cut from the hole so as to be of suitable size for SEM examination. The specimen was ultrasonically cleaned with trichloroethylene. After cleaning, some of the dark product had come off; still, many areas with surface residue could be observed in the SEM.

3. RESULTS

Figure 3 presents a low-magnification montage of three SEM photographs. The hole edge is on the right. This figure suggests that the fatigue crack originated from the region at the bottom right edge. Various areas were magnified (Fig. 4), fatigue striations could be readily identified, and their orientation pointed to the region at the bottom right edge of Fig. 3 as the initiation point.

Attempts to examine the details of the edge at the hole (i.e., perpendicular to the arrow in Fig. 3) were unsuccessful, because the hole had many machining marks (presumably produced during cutting of the specimen to open the crack or later). Hence, the precise initiation point could not be located.

In addition to striations, many areas where the fatigue features were either absent or masked were also observed (Fig. 5). Nondispersive X-ray examination of some of the corroded areas indicated the presence of Al, Zn, and Cu, all three elements present in 7075 alloy (Fig. 6a). By comparison with spectra from a mixture of equal amounts of NaCl and Na_2SO_4 (Fig. 6b) the presence of chlorine and sulfur is also confirmed in the spectra (Fig. 6a) from the corroded area. Frequently very small peaks of elements identified as silver and cadmium were observed in various areas; no source for these can be suggested.

4. DISCUSSION

The observed crack was definitely due to fatigue--fatigue striations were readily visible over the total crack surface (e.g., Fig. 7 is nearly three-fourths the way from the initiation region to overload region) except at the end where overload features were observed. These were presumably caused by the opening up of the crack from the other end (away from the hole). The exact cause of the fatigue origin cannot be determined. Stress corrosion initiation at the edge is ruled out because the crack originated at or very close to the edge and no stress corrosion features were recognizable. The most probable cause seems to be a machining notch at the initiation point in the hole, although initiation at a possible inclusion is not completely excluded by our observations. However, no inclusion, or cavity from which an inclusion may have dropped out, was observed at or near the suspected initiation point. Indeed, the fact that inclusions were very hard to find on most of the fatigue surface suggests that this region came from relatively clean alloy.

Finally, the corrosive environment attacked certain areas, masking or obliterating fatigue features at these locations. Since many more clean areas exhibiting fatigue features could be observed over the whole crack surface, it is concluded that the role of corrosion in initiating and propagating this crack was very small, if any. The results suggest that the crack would have also originated or propagated in the absence of the corrosive environment.

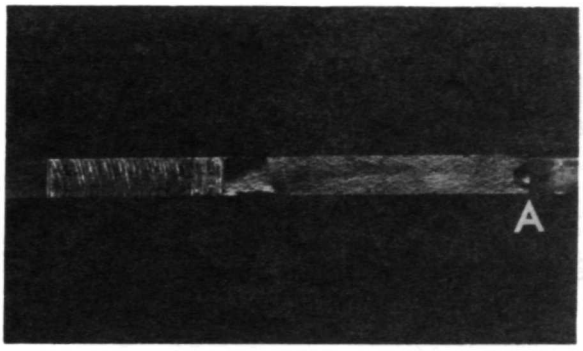

Mag. 3/4X

Figure 1

The Bomb Rack Plate in the Condition Received by IITRI. A is the edge near the hole where the fracture initiates.

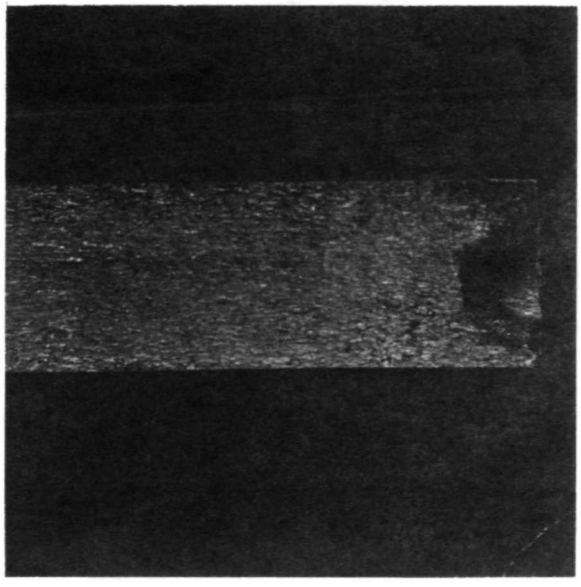

Mag. 4X

Figure 2

An Enlarged View of Area Near A. Notice the dark corrosion products on the right.

Mag. 27X

Figure 3

Composite SEM Photographs of Edge A (of Fig. 1)
Suggesting Initiation from the Lower Right Edge.

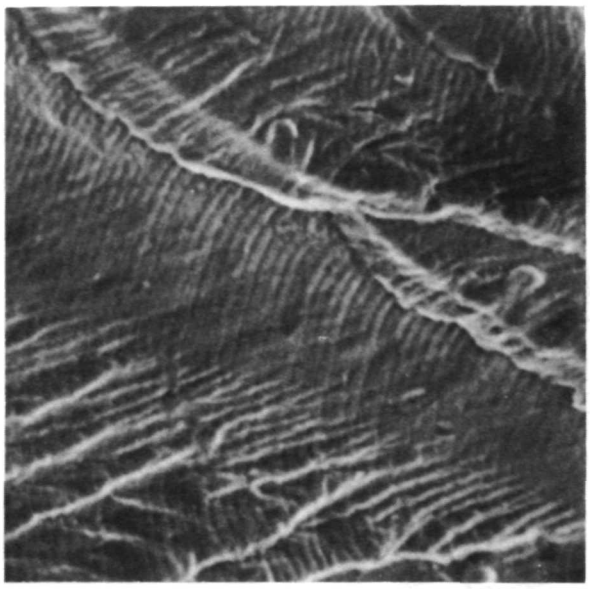

Mag. 2700X

(a)

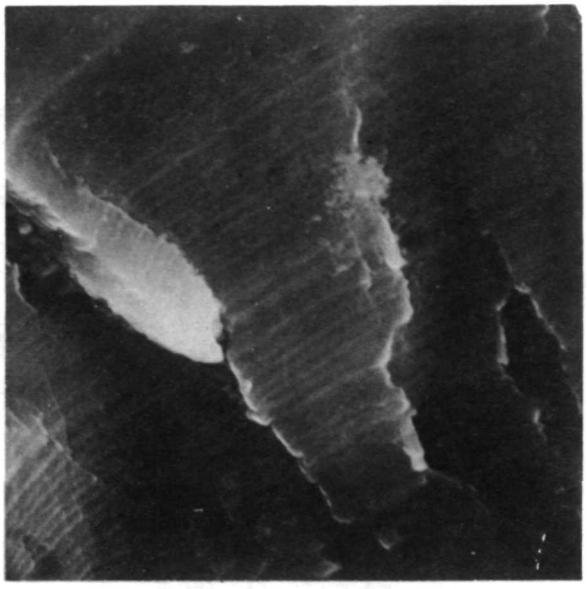

Mag. 3000X

(b)

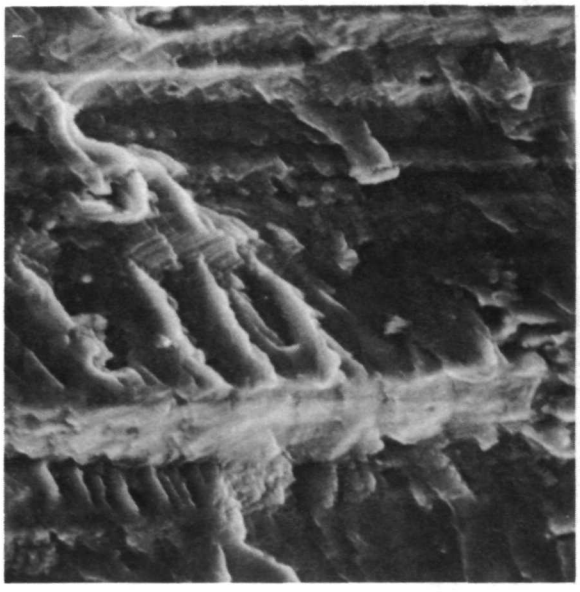

Mag. 480X

(c)

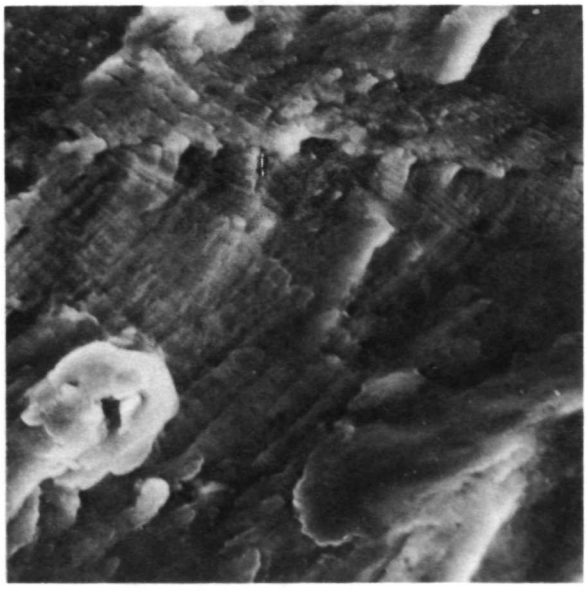

Mag. 1000X

(d)

Figure 4

(a) Area W, (b) Area X, (c) Area Y, and (d) Area Z of Fig. 3 at High Magnification.

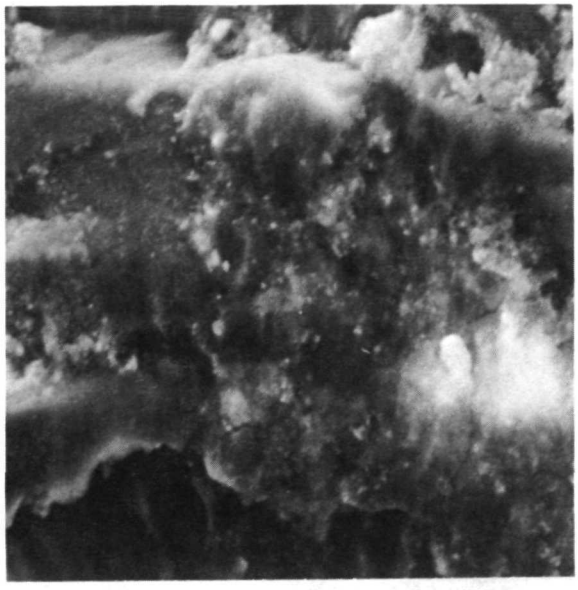

Mag. 600X

(a)

Mag. 2700X

(b)

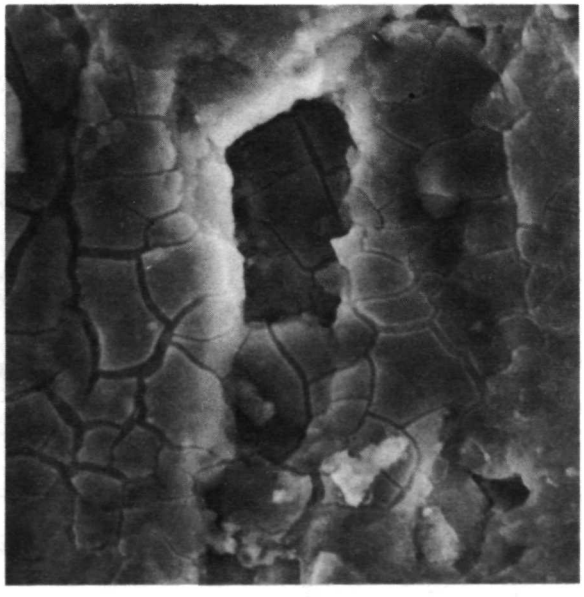

Mag. 1000X

(c)

Figure 5

Corrosion Debris at Various Locations on the Fracture Face in Fig. 2.

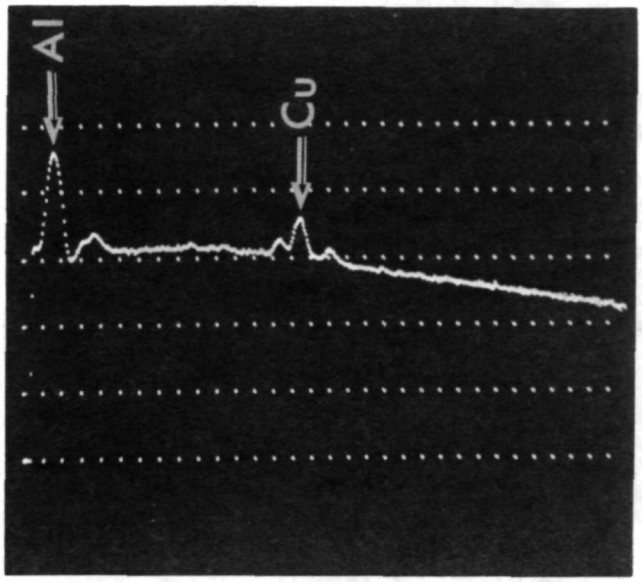

(a)

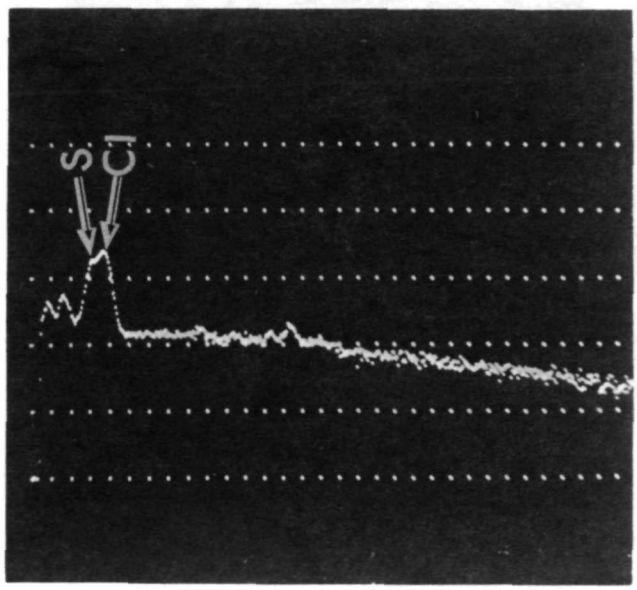

(b)

Figure 6

Analysis of Corrosion Debris (Figure 5c). (a) X-ray spectrum; (b) standard spectrum from NaCl and Na_2SO_4 mixture indicating the nature of peak when sulfur and chlorine are present together.

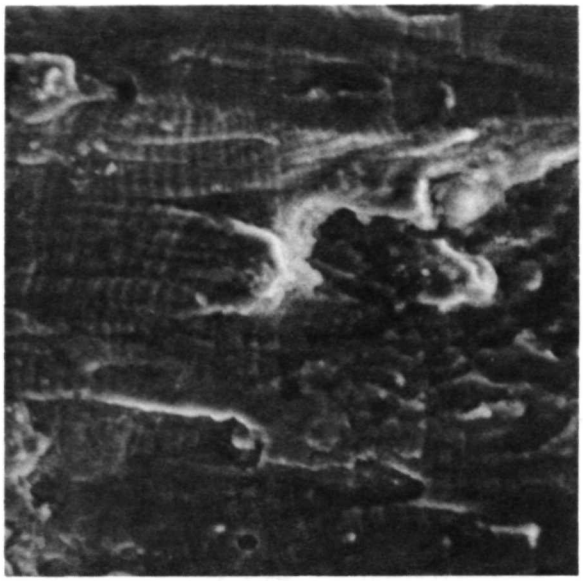

Mag. 770X

(a)

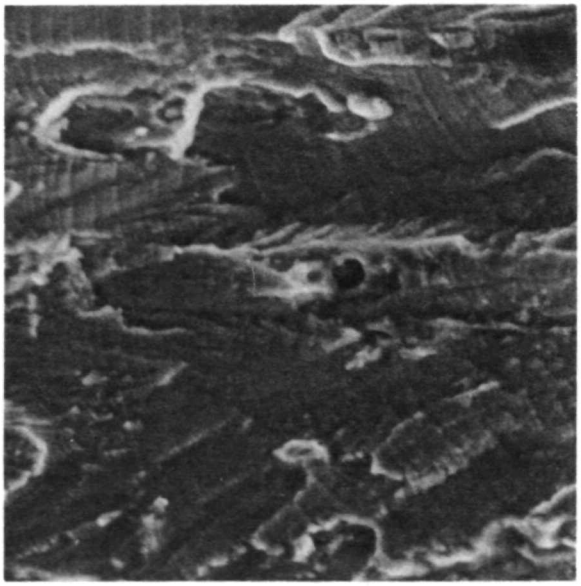

Mag. 770X

(b)

Figure 7

Fatigue Features at About 3/4 the Distance from the Initiation Edge to the End of the Fatigue Crack.

APPENDIX VI

FAILURE ANALYSIS OF ALUMINUM ALLOY COMPONENTS--SAMPLE VI

1. INTRODUCTION

This report presents our analysis of a failure in a propeller hub. The sample for failure analysis was supplied by the Air Force Materials Laboratory. The piece obtained by IITRI (Fig. 1a) had shown cracks during nondestructive testing, and had already been opened up by AFML for their analysis. The material was 2014 aluminum alloy in the T-6 condition.

2. EXPERIMENTAL

Visual and low-magnification examination in a binocular microscope showed the presence of corrosion products on the fracture surface, and propagation patterns similar to those for fatigue fractures originating at the root of the thread. In Fig. 1c, area A is the thread surface, B is the crack surface, C is the saw cut surface, and D identifies overload regions formed during the opening of the crack.

The sample was cut to a size suitable for direct examination in the SEM. The piece was then ultrasonically cleaned in acetone and trichloroethylene. The residue on the crack surface did not come off during this operation, and further cleaning with a nylon brush and Freon solvent was also unsuccessful in removing the debris. In many areas the film had a brownish appearance, which was subsequently analyzed by the energy dispersive X-ray method on the SEM.

The root of another thread was also examined. Low-magnification optical microscope examination (Fig. 2) revealed the presence of many cracks. A small area of this root was opened up, and it showed patterns similar to those observed on the main crack surface shown in Fig. 1c.

3. RESULTS

Figure 2a shows a low-magnification SEM view of one of the typical areas of the crack surface. Areas close to the overload region (B) appeared relatively clean and were progressively magnified (Fig. 2b, c, d). Although considerable debris was present, crack propagation by fatigue was confirmed. Figure 3 presents four views of another similar area. Again, the crack initiation was at root of the thread (A), and propagation by fatigue (B) was confirmed. The results also indicate the presence of a severe corrosive environment (C).

X-ray examination of the brownish debris (e.g., brightness in Fig. 4) indicated the presence of Si, Fe, and Ca in addition to Al (Fig. 5). The presence of these elements was repeatedly noted though their intensities varied from area to area. Thus, in the left part of Fig. 5, Fe is predominant, followed by lesser amounts of Ca and Al-Si (these elements are not resolved when simultaneously present). In the right part of Fig. 5 the Fe and Al-Si peaks were of about the same intensity in another area. The residue thus appears to consist of complex silicates of Fe, Ca, and Al.

Figure 6a shows cracking at a thread root (compare with Fig. 2). The same crack is observed to be continuous at the root; e.g., see leftward continuation of Fig. 6a in Fig. 6b. Corrosive environment has severely attacked the metal in many areas, and indications of pitting (Fig. 6c) as well as spalling (Fig. 6d) are evident all over the thread root. When this root was opened up, the features revealed were identical to those reported above (Figs. 2 to 5). No evidence of shot peening to reduce unfavorable stress patterns at the root was found.

4. DISCUSSION

The crack observed at the thread root in Fig. 1c initiated at many points along the root of the thread. Growth from each initiation point continued until two propagating crack

fronts joined each other, usually forming a ridge (since the initial crack propagation from different fronts was not all in the same plane). This resulted in the appearance observed in Fig. 1c.

The initiation of cracks at various points along the root may result from the presence of machining notches or from pits and spalls caused by corrosion. Due to their narrower cross section, the roots already have a higher stress concentration, which may accelerate corrosive processes. Stress-corrosion effects may also be operative in crack initiation, particularly where certain areas fell out of the thread root due to preferential attack at grain boundaries and thus further enhanced the stress concentration effects.

Once the cracks initiated, the propagation was predominantly due to fatigue, since the areas which were farthest from the origins were relatively clean (in particular see the clear striations on the left of Figs. 2d and 3c). However, corrosion of the already fractured surface continued (e.g., see right of Fig. 3d), though the rate of attack was slower at the areas farthest from the initiation points. The specific nature of the corrosive environment cannot be inferred from knowledge only of the presence of Fe, Si, and Ca on the cracked surface.

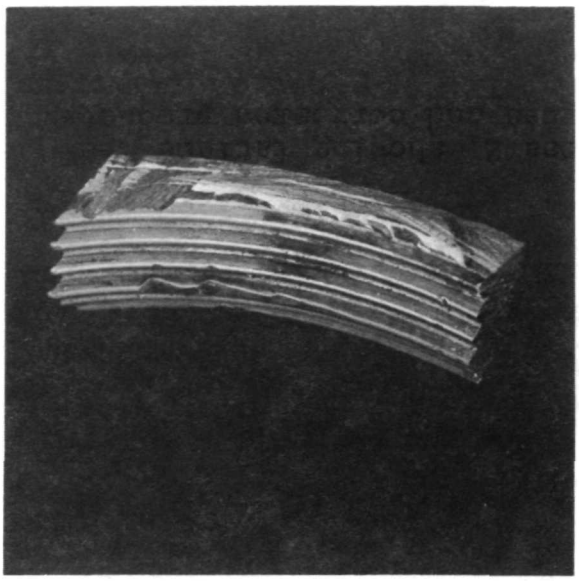

(a) 2/3X

Specimen as received by IITRI

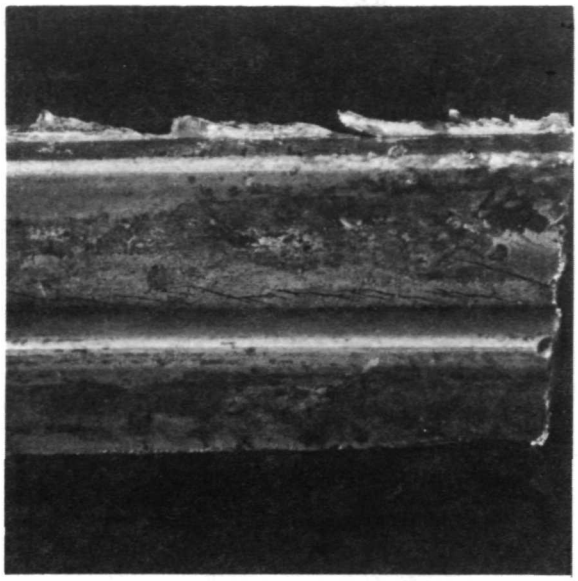

(b) 6X

Details of a thread root from Fig. 1a.

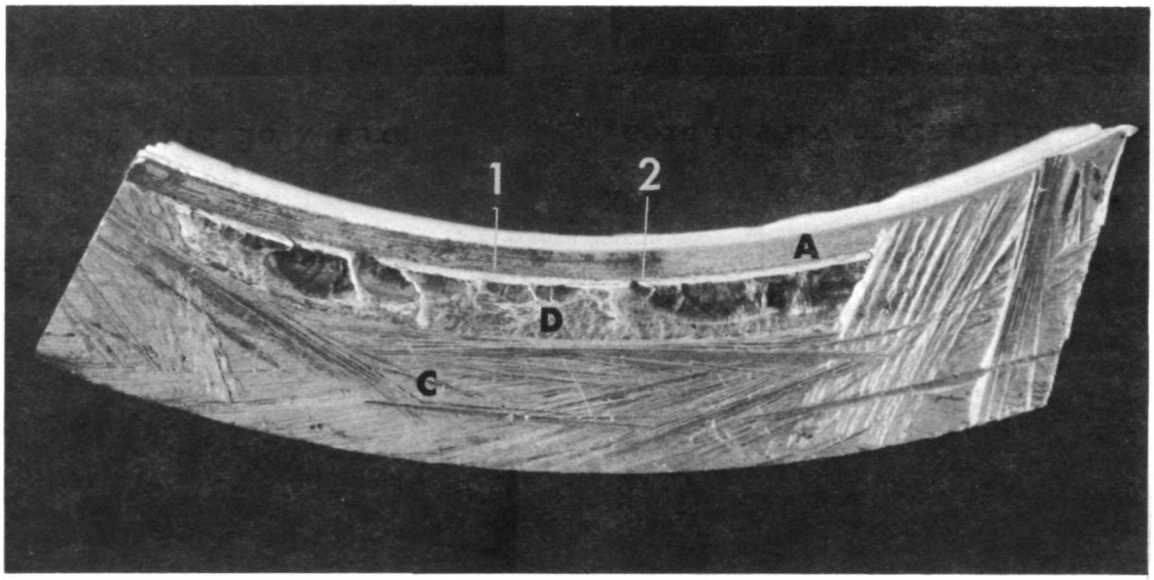

(c) 5X

Opened up crack area, showing thread surface (A), crack surface (B), saw cutting marks (C), and overload region (D). Details of areas 1 and 2 are presented in Figs. 2 and 3.

Figure 1

Optical Photomacrographs of Failure in Propeller Hub.

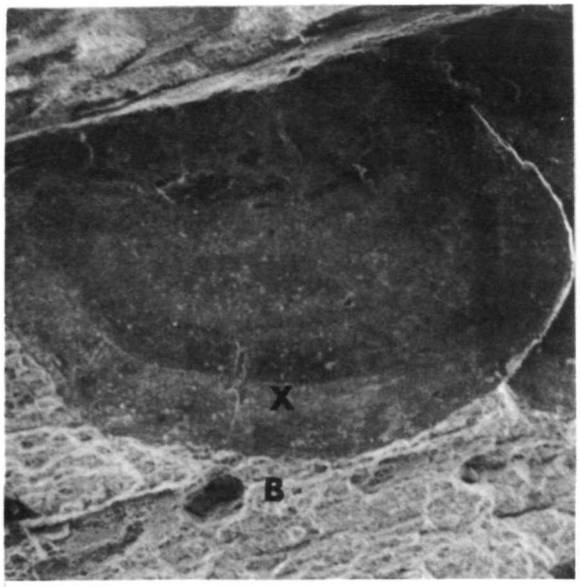

(a) 60X

Low-magnification view of area.

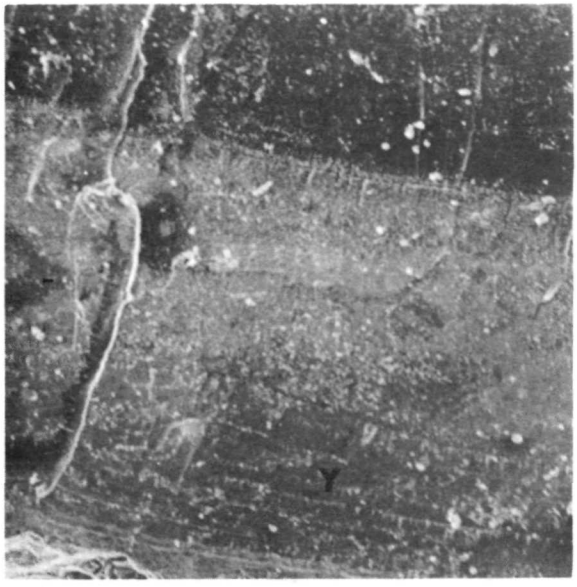

(b) 360X

Area X of Fig. 2a.

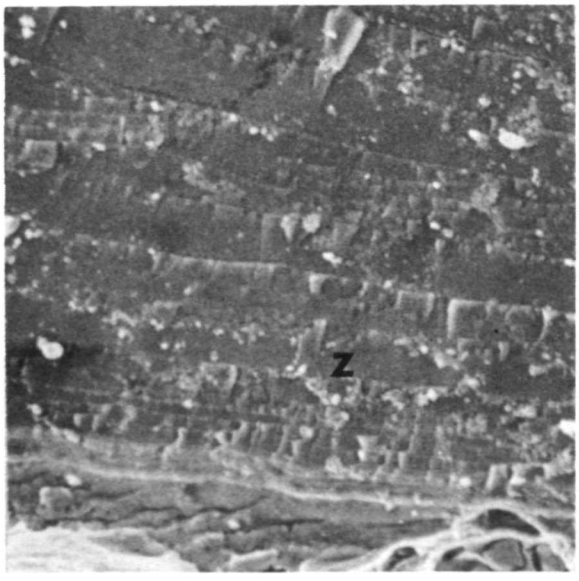

(c) 1100X

Area Y of Fig. 2b.

(d) 3600X

Area Z, showing fatigue features and corrosion products.

Figure 2

SEM Fractographs of Area 1 in Fig. 1c.

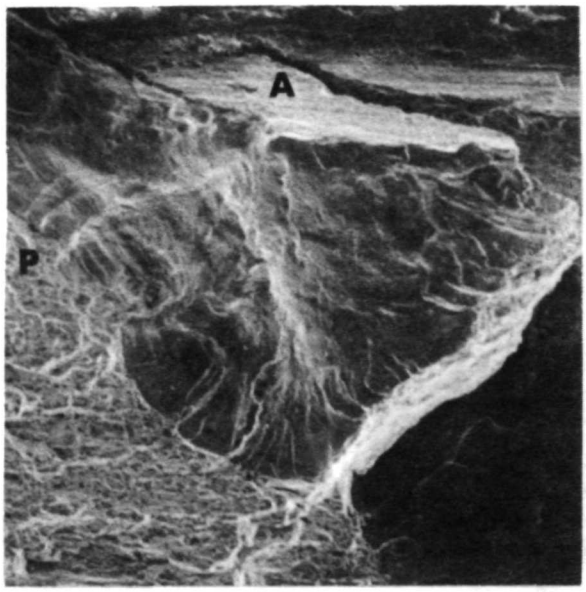

(a) 50X

Low-magnification view of area.

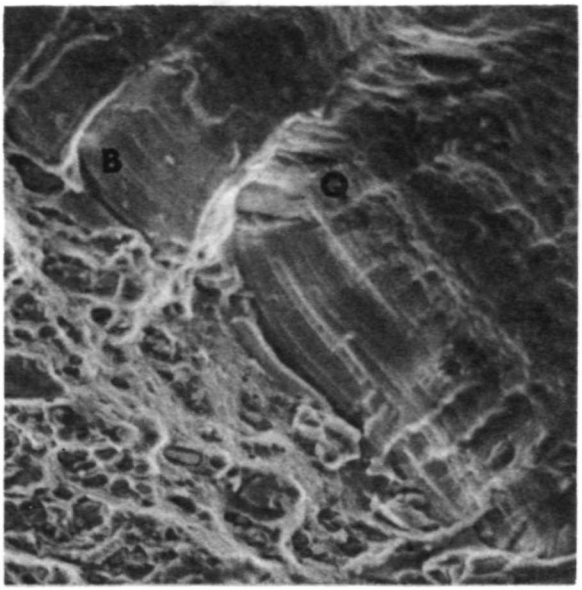

(b) 180X

Region P of Fig. 3a.

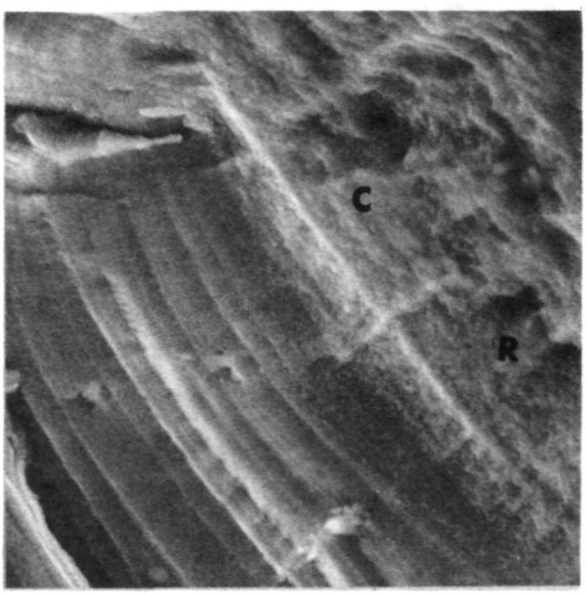

(c) 600X

Region Q of Fig. 3b.

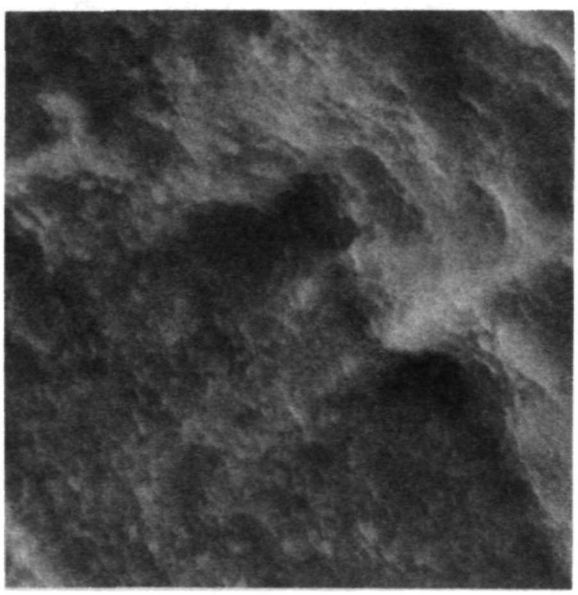

(d) 1800X

Region R of Fig. 3c.

Figure 3

SEM Fractographs of Area 2 in Fig. 1c, Showing Fatigue Features and Corrosion Attack.

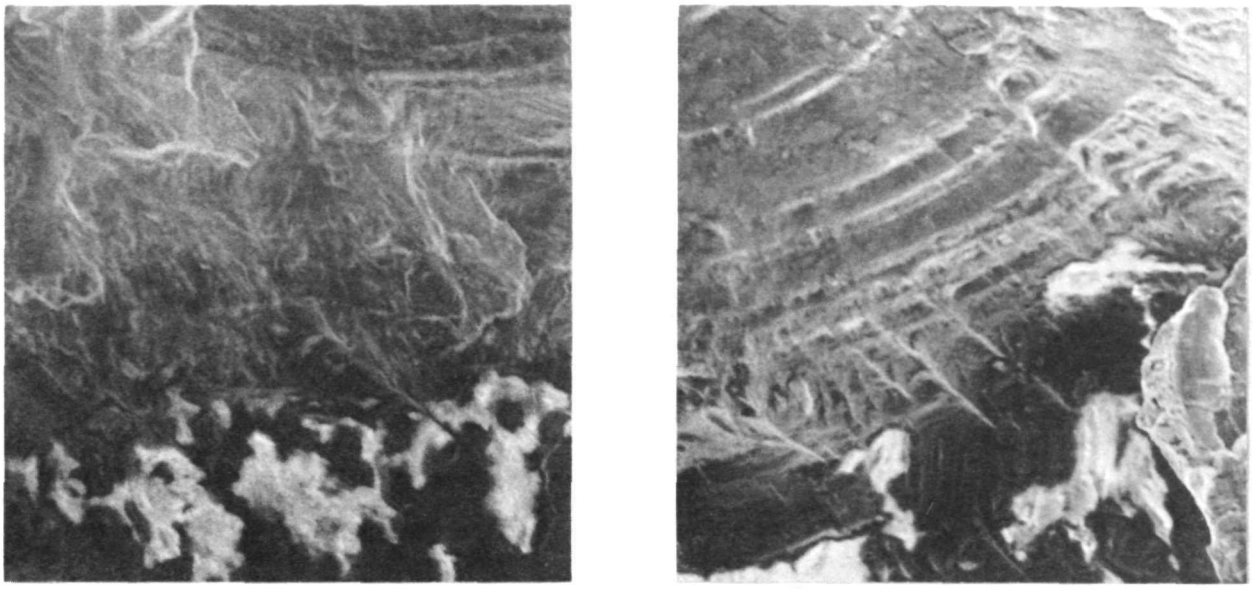

(a) 36X (b) 60X

Figure 4

SEM Photographs of Initiation Region of Another Crack. Very bright areas are brownish debris visible under optical microscope.

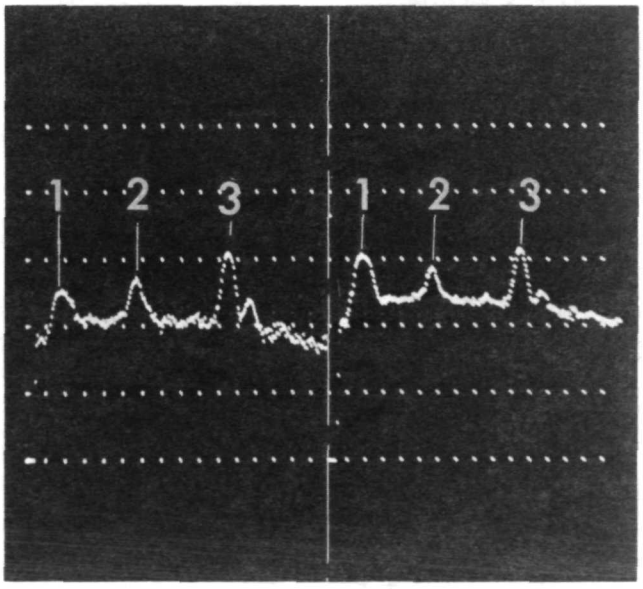

Figure 5

X-Ray Analysis of Two of the Debris Areas. Peaks in both patterns from left to right are (1) mixture of Al and Si, (2) Ca, and (3) Fe.

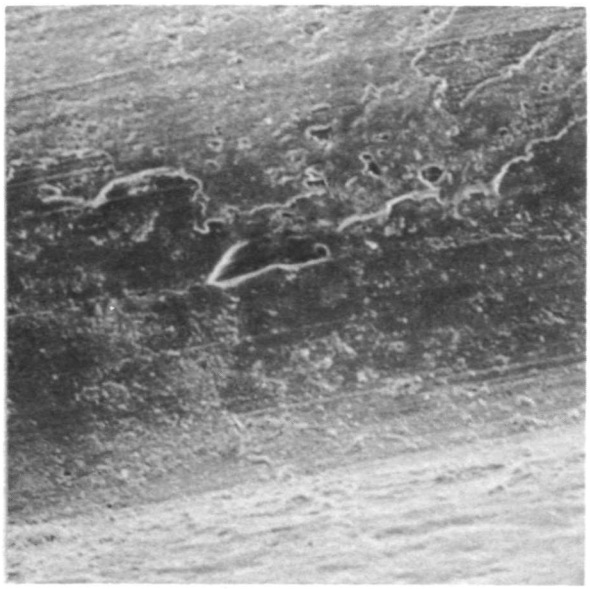

(a) 60X

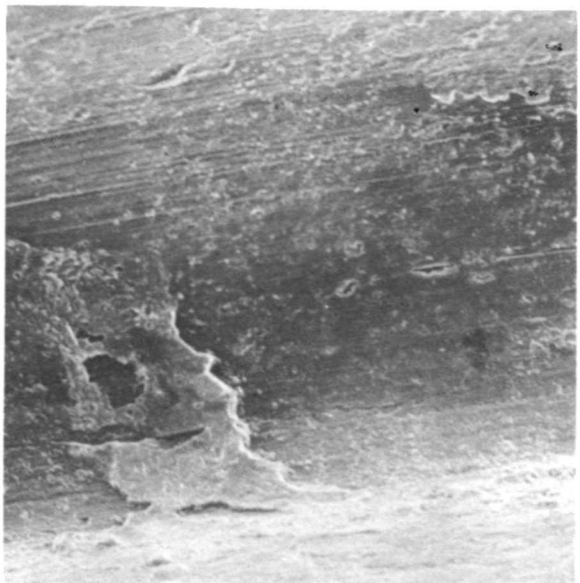

(b) 60X

Region at left of Fig. 6a, indicating continuation of crack.

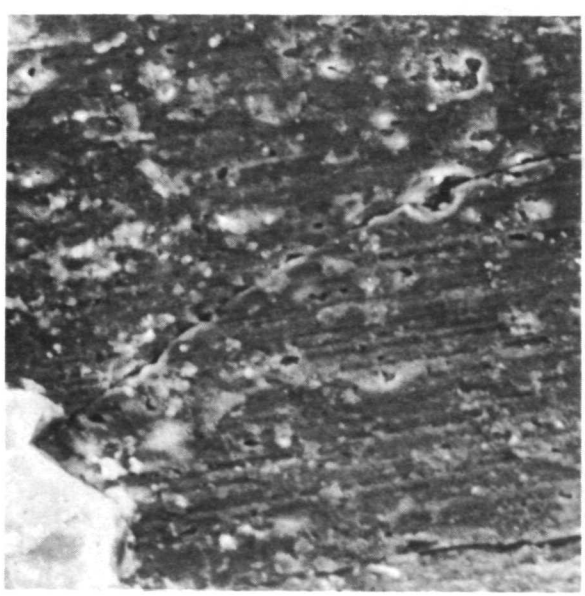

(c) 180X

(d) 300X

Center of Fig. 6a.

Figure 6

SEM Details of the Thread Root Surface (Fig. 1b).

REFERENCES

1. O. Johari, "Microstructure with the SEM--A New Approach Through SEM Fractography," Electron Microscopy and Structure of Materials, University of California Press, Berkeley, pp. 313-332, September 1971.

2. IITRI Program B8129, "A Handbook of Failure Analysis of Metallic Materials by Scanning Electron Microscopy," IIT Research Institute, Chicago, to be published late 1972.

3. O. Johari, "Comparison of Transmission Electron Microscopy and Scanning Electron Microscopy of Fracture Surfaces," J. Metals, pp. 26-32, June 1968.

4. W. A. Sipes, Naval Air Development Center, Report No. NADC-MA-7061, October 1970 (AD 875653L).

5. W. Rosenhain, "The Microscopic Examination of Metals," in An Introduction to the Study of Physical Metallurgy, D. Van Nostrand Company, New York, p. 16, 1915.

NASA-Langley, 1973 —— 17 CR-2166

NATIONAL AERONAUTICS AND SPACE ADMINISTRATION
WASHINGTON, D.C. 20546

OFFICIAL BUSINESS
PENALTY FOR PRIVATE USE $300

SPECIAL FOURTH-CLASS RATE
BOOK

POSTAGE AND FEES PAID
NATIONAL AERONAUTICS AND
SPACE ADMINISTRATION
451

U.S.MAIL

POSTMASTER: If Undeliverable (Section 158 Postal Manual) Do Not Return

"The aeronautical and space activities of the United States shall be conducted so as to contribute . . . to the expansion of human knowledge of phenomena in the atmosphere and space. The Administration shall provide for the widest practicable and appropriate dissemination of information concerning its activities and the results thereof."

—NATIONAL AERONAUTICS AND SPACE ACT OF 1958

NASA SCIENTIFIC AND TECHNICAL PUBLICATIONS

TECHNICAL REPORTS: Scientific and technical information considered important, complete, and a lasting contribution to existing knowledge.

TECHNICAL NOTES: Information less broad in scope but nevertheless of importance as a contribution to existing knowledge.

TECHNICAL MEMORANDUMS: Information receiving limited distribution because of preliminary data, security classification, or other reasons. Also includes conference proceedings with either limited or unlimited distribution.

CONTRACTOR REPORTS: Scientific and technical information generated under a NASA contract or grant and considered an important contribution to existing knowledge.

TECHNICAL TRANSLATIONS: Information published in a foreign language considered to merit NASA distribution in English.

SPECIAL PUBLICATIONS: Information derived from or of value to NASA activities. Publications include final reports of major projects, monographs, data compilations, handbooks, sourcebooks, and special bibliographies.

TECHNOLOGY UTILIZATION PUBLICATIONS: Information on technology used by NASA that may be of particular interest in commercial and other non-aerospace applications. Publications include Tech Briefs, Technology Utilization Reports and Technology Surveys.

Details on the availability of these publications may be obtained from:

SCIENTIFIC AND TECHNICAL INFORMATION OFFICE

NATIONAL AERONAUTICS AND SPACE ADMINISTRATION

Washington, D.C. 20546